AN ABSTRACT OF THE THESIS OF

Chia-Jen Chen for the degree of Master of Science in Chemical Engineering presented on July 2, 1997. Title: A Study of ZnS:Mn Electroluminescent Phosphors Grown by Halide Transport Chemical Vapor Deposition

Redacted for Privacy

Abstract approved: _____

Milo D. Koretsky

A low pressure halide transport chemical vapor deposition (HTCVD) system to grow ZnS:Mn electroluminescent phosphors is characterized. Reactor parameters such as gas composition, gas flow rate, and source and substrate temperature are investigated. Crystal structure is investigated using x-ray diffraction, electron spin resonance, and transmission electron microscopy. Chemical characterization includes electron microprobe and Auger electron spectroscopy. Double-insulating alternating current thin film electroluminescent devices are constructed around the HTCVD phosphors. The devices are studied using electroluminescence (brightness-voltage), photoluminescence and electrical characterization.

The luminescent properties of films with a (002) preferred orientation are studied. A maximum electroluminescent brightness of 1475 cd/m^2 is achieved. The photoluminescence (PL) of ZnS:Mn films grown at different substrate temperatures is compared. The intensity correlates to Mn concentration. Red emission is seen in films grown at lower substrate temperature which have low Mn concentration. Mechanisms

proposed in the literature cannot explain the red emission. A blue PL ZnS film intentionally doped with chlorine is achieved. This blue emission is associated with self-activated (SA) emission.

Hexagonal and cubic thin-film ZnS:Mn electroluminescent phosphors are grown by HTCVD. Processing conditions, most notably introduction of a H_2S ambient, lead to a change in the preferred orientation and phase of the polycrystalline thin film. In addition to the commonly reported growth along the closest packed plane [(111) for cubic crystal structure or (002) for hexagonal], thin films have been grown along the less dense cubic (311) direction.

The electrical characterization of ZnS:Mn ACTFEL devices with phosphors having different structure and preferred orientation is studied. A comparison of different preferred orientations and structures on conduction charge, obtained by internal charge-phosphor field ($Q\text{-}F_p$), is performed. When grown in the (311) direction, the conduction charge of a ZnS:Mn ACTFEL device increases from 2.3 $\mu C/cm^2$ to 5.0 $\mu C/cm^2$. Moreover, the leakage charge, Q_{leak}, of the (311) HTCVD films is small compared to other devices.

A Study of ZnS:Mn Electroluminescent Phosphors Grown by Halide Transport Chemical Vapor Deposition

by

Chia-Jen Chen

A THESIS

submitted to

Oregon State University

in partial fulfillment of
the requirements for the
degree of

Master of Science

Presented July 2, 1997
Commencement June 1998

Master of Science thesis of Chia-Jen Chen presented on July 2, 1997

APPROVED:

Redacted for Privacy

Major Professor, representing Chemical Engineering

Redacted for Privacy

Head or Chair of Department of Chemical Engineering

Redacted for Privacy

Dean of Graduate School

I understand that my thesis will become part of the permanent collection of Oregon State University libraries. My signature below authorizes release of my thesis to any reader upon request.

Redacted for Privacy

Chia-Jen Chen, Author

ACKNOWLEDGMENT

I could not have finished without the help and support of many others who each contributed to the effort in one way or another. I would like to take this opportunity to express the great appreciation to:

My advisor, Dr. Milo D. Koretsky, for his great patience, support, guidance and idea throughout my study in Oregon State University.

Dr. John F. Wager and Dr. Tom Plant for many fruitful discussion, the opportunity to join their research group meeting, and the use of their facilities.

Sjamsie Husurianto and Xiaobin Lu, for all of the assistance in the lab.

Dr. Pat Woodward, Ju-Zhou Tao, Dong Li, and Kam-Fai So for assistance in using their facilities, good discussion and patience with my many questions.

Dr. Paul H. Holloway and Dr. Christopher J. Summers for the resources provided by the Phosphor Technology Center of Excellence.

Art Neeley, Leon Ungier, and P. Nick Wannemacher for their technical assistance.

The rest of the Koretsky, Wager and Dr. Arthur W. Sleight research group, for many help.

My family, whom I love, for dealing so well with my desire to live so far away from home.

This work was supported by the Advanced Research Projects Agency under the Phosphor Technology Center of Excellence, Grant No. MDA 972-93-1-0300.

TABLE OF CONTENTS

TABLE OF CONTENTS (Continued)

LIST OF FIGURES

LIST OF FIGURES (Continued)

LIST OF FIGURES (Continued)

LIST OF TABLES

Dedicated to my parents

A Study of ZnS:Mn Electroluminescent Phosphors Grown by Halide Transport Chemical Vapor Deposition

Chapter 1

Introduction

Flat panel displays are an attractive alternative to cathode-ray tubes (CRTs) for visual display applications due to their planar geometry and portability. The four main types of flat panel displays include: liquid crystal displays (LCD), electroluminescent (EL) displays, field emission displays (FED) and plasma display panels (PDP). Liquid crystal displays have dominated the computer monitor market in recent years. However, EL displays offer many advantages when compared to LCDs, such as: high brightness, high contrast, wide viewing angle, fast response time, and thermal and mechanical stability. There are four types of EL display configurations: alternating-current thin-film EL (ACTFEL), alternating-current powder EL, direct-current thin-film EL and direct-current powder EL. Both organic and inorganic phosphor materials are being investigated. Among these configurations, inorganic ACTFEL displays are currently best suited for commercial application due to their long lifetime and durability. Monochrome manganese-doped zinc sulfide (ZnS:Mn) ACTFEL displays, which emit yellow-orange light, were introduced into the market place in 1983. Recently, full-color EL displays have also been developed.

Several challenges remain in commercializing ACTFEL devices, including development of better growth processes and obtaining a more complete understanding the

relationship between crystal structure, composition, luminescence and device operation. One processing difficulty is the demand for the production of a uniform thin film across the entire monitor display area, which can be 14 inches in diagonal or larger. Better crystal quality, easily controllable dopant amounts, and low contamination in films are other challenging factors toward obtaining better EL displays.

Another problem regarding ACTFEL development is the incomplete understanding of the relation of crystal structure and composition to luminescence and device operation. Although dopant concentration is realized as a major factor in EL performance, the importance of the structure and composition of the host material on device stability has been neglected until recent years. The structural deformations (defects) associated with the ZnS host material, such as zinc or sulfur vacancies, on the influence of luminescent property and stability are not so clear. Further investigation of the local structure around the luminescent center and structural defects from aging is necessary.

The goal of this study is to investigate 1) the structural and chemical characteristics of ZnS:Mn thin films grown by halide transport chemical vapor deposition (HTCVD), 2) the effect of substrate temperature and luminescent impurities on luminescent properties, and 3) the effect of structure and orientation on the electrical characteristics of ZnS:Mn ACTFEL devices.

The thesis is organized as follows. Chapter 2 presents a review of previous literature including: the deposition methods for growing ZnS:Mn thin films, structural and chemical characterization of these films, and luminescent properties and electrical

characterization of ZnS:Mn ACTFEL devices. Chapter 3 describes the experimental procedure and operational conditions used in this study. Chapter 4 discusses the growth and chemical characteristics of ZnS:Mn films prepared by halide transport chemical vapor deposition. Chapter 5 presents the effect of substrate temperature, impurities and defects on the luminescent properties of ZnS:Mn devices. Chapter 6 discusses the relation of the structure of ZnS:Mn to its electrical characteristics. Chapter 7 presents the conclusions of this study and recommendations for future work.

Chapter 2

Literature Review

2.0 The ZnS:Mn ACTFEL Device

2.1 Brief History

Manganese-doped ZnS has been the most promising light-emitting material studied in the development of ACTFEL devices because of its high stability and brightness. The first ZnS:Mn thin-film EL device was developed in the late 1950's by Vlasenko [1960]. However, commercial application was precipitated by the introduction of the double-insulating layer structure presented by Inoguchi et al. [1974] at the 1974 SID International Symposium. The authors demonstrated the high luminescence of this ZnS:Mn ACTFEL device and stability for more than 10,000 hours of operation. Since then, much effort has been devoted to the improvement of the device by applying different growth methods, including chemical and physical vapor deposition, to deposit high quality ZnS:Mn thin films.

The first 6 inch-diagonal matrix monochrome ZnS:Mn EL display was introduced to the market in 1983 [Takeda, 1983], and the 9-inch display, in the mid 80's. After that, the development of ACTFEL displays for practical production have grown very rapidly.

Since the mid-1980's, more extensive studies have focused on investigating new phosphor materials for the three primary colors (red, green and blue) for developing a

full-color ACTFEL display to fit market requirements. In 1994 the full-color thin-film EL display monitor with 320 x 256 pixels was developed and produced [Barrow, 1994]. In order to improve the efficiency of full-color display, more fundamental studies have been pursued, including the basic physics of ACTFEL devices and the phenomenon of aging. Many of these studies have focused on ZnS:Mn thin films due to its commercial importance.

2.2 Structure of the Device

The structure of a typical ZnS:Mn ACTFEL device is shown in Figure 2-1. It consists of a ZnS:Mn phosphor film sandwiched between two insulating layers. Additional conductors comprise the top and bottom layers. These five films are grown on a corning 7059 glass substrate. The two conducting layers are used as electrodes. The insulating layers are applied to protect the phosphor layer from electrical breakdown. High transmittance is necessary for the bottom electrode and insulating layer to allow the visible light emitted from the ZnS:Mn phosphor layer to pass through.

The phosphor layer consists of zinc sulfide host material and manganese luminescent centers. ZnS is a wide band gap (3.6 eV) II-VI semiconductor material which provides a host for emission of visible light without absorption and allows high energy electron transport. The emission originates from radiative transition between local states of Mn luminescent centers.

A thin film of indium-tin-oxide (ITO) is most commonly used for the bottom electrode in the ACTFEL device due to its conductivity and high transparency. Aluminum is generally used for the top electrode. In order to protect the ZnS:Mn phosphor layers from electric breakdown while a high electric field (1.5 MV/cm) is applied across phosphor, an insulating layer consisting a high dielectric breakdown electric field and small number of defects is necessary. The insulator should also have a high dielectric constant to minimize the energy loss across this layer. Finding materials with both a high dielectric constant and high breakdown electric field is challenging. Many different insulating materials, such as aluminum-titanium oxide (ATO), silicon oxynitride (SiON), Y_2O_3, barium tantalate ($BaTiO_3$) (BTO), and Si_3N_4 have been used [Ono, 1995]. In this study, the ATO and SiON are used as the bottom and top insulating layers, respectively. The typical thicknesses for individual layers are indicated in Figure 2-1.

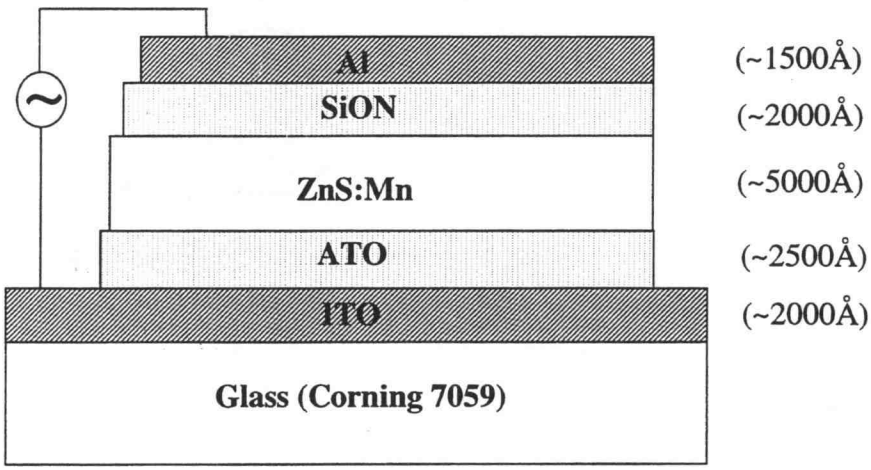

Figure 2-1 The ZnS:Mn ACTFEL device structure used in this work.

2.3 Device Operation

Energy input to the ZnS:Mn EL device is provided by applying an AC voltage to the two electrodes. The driving waveform used in this work is a bipolar pulse with a 5 μs rise/fall time, pulse width of 30 μs, and a frequency of 1 kHz. The device is typically driven at 20, 40 and 60 V above the threshold voltage for electrical characterization.

Figure 2-2 shows the energy band diagram when a negative bias is applied to the Al electrode, causing the slope shown in the energy band diagram.

The EL emission mechanism is generally understood in the following way. Below the threshold voltage, electrons are stored at the interface of the insulating and phosphor layer. When the voltage is higher than the threshold voltage (V_{th}), the phosphor layer breaks down and the electrons start tunneling out of the interface and drift across the phosphor layer. The charge transported across the phosphor during the voltage pulse is called conduction charge (Q_{cond}). As the electrons transport through the phosphor, they are accelerated and gain kinetic energy in the high electric field. Electrons with sufficient kinetic energy release some energy to the luminescent centers upon impact. This excites electrons of the Mn luminescent centers from the $3d^5$ ground state to the local excited states. Light emission is generated through radiative de-excitation. After the positive wave form, the electrons get trapped at the other phosphor/insulator interface, causing charge polarization. The stored charge at the interface prior to the opposite polarity is called polarization charge (Q_{pol}). When the positive bias is applied to the Al electrode, the process describe above takes place in the opposite direction. During the zero voltage

portion of the wave form, electrons may leak back to the phosphor from shallow interface state, giving rise to the so called leakage charge (Q_{ieak}).

Space charge may also be created within the phosphor. This is represented by a change in the slope of the energy bands (Figure 2-2). Many explanations have been proposed for space charge, such as the existence of defects, impact ionization, and hole capture [Abu-Dayah, 1993; Douglas, 1993]. Anomalous electrical characteristics of EL devices have be explained by including space charge [Abu-Dayah, 1993; Shih: 1995, 1996].

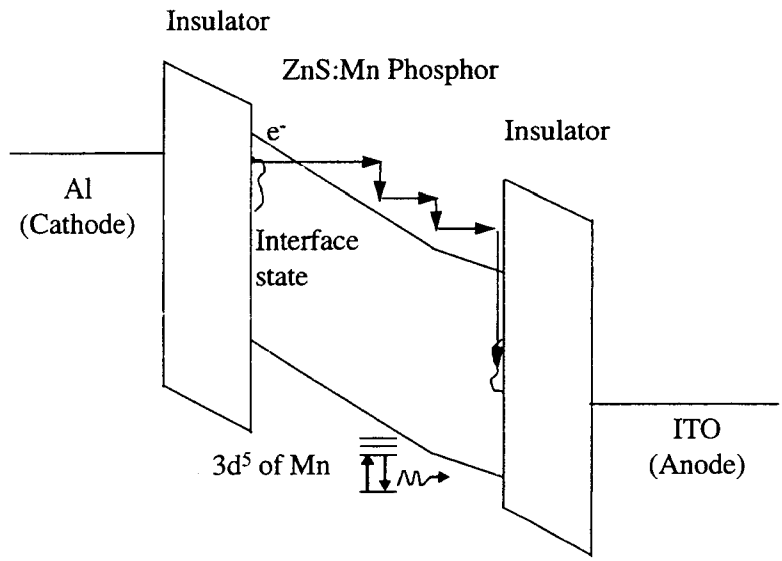

Figure 2-2. Energy band diagram of the ACTFEL device with a negative bias applied to the Al electrode.

2.4 ZnS:Mn Thin Film Fabrication

In order to improve device characteristics such as increased luminance, stability, and to decrease processing costs for ZnS:Mn, many different deposition methods for ZnS:Mn have been studied. These techniques include: electron beam evaporation (EBE) [Hurd, 1979; Ono, 1995], thermal evaporation [Ono, 1995], sputtering [Xian, 1994], multi-source deposition (MSD) [Nire, 1994], atomic layer epitaxy (ALE) [Suntola, 1992], metalorganic chemical vapor deposition (MOCVD) [Migita, 1988], and halide-transport chemical vapor deposition (HTCVD) [Mikami, 1991]. Controllable dopant concentration, proper stoichiometry, high crystallinity, and uniformity are major concerns. Among these methods, physical vapor deposition methods (e.g., EBE, thermal evaporation, sputtering, and MSD) provide high deposition rate and low substrate temperature. On the other hand, the films grown by chemical vapor deposition methods (e.g., ALE, MOCVD, and HTCVD) are prepared at a higher substrate temperature and a lower deposition rate, but with better crystallinity and higher luminous efficiency.

Until now, ZnS:Mn ACTFEL displays have been commercially prepared by EBE and ALE. ALE produces films with good crystal quality, large grain size (100 nm), and columnar grain growth. The grain size in EBE films is only 25 nm [Ono, 1995; Theis, 1983], although the size can be increased by post annealing. However, ALE is expensive and requires longer deposition time.

Device performance is influenced by selection of source materials which may leave undesirable impurities in the films. In ALE, Zn source materials include: $ZnCl_2$,

$Zn(CH_3COO)_2$ and $Zn(thd)_2$ (where thd is 2,2,6,6,-tetramethy-3,5-heptanedione) and while Mn source materials are $MnCl_2$ and $Mn(thd)_2$. Chlorine has been detected in ALE-deposited ZnS:Mn from chlorine based precursors. Chlorine is mobile under large electric fields and can lead to changes of device performance with time (aging). The precursors used in MOCVD include $Zn(CH_3)_2$, $Zn(C_2H_5)$, TCM [$(CH_3C_5H_4)Mn(CO)_3$: tricarbonyl methylcyclopentadienyl manganese] and CPM [$(C_5H_5)_2Mn$: di-π-cyclopentadienyl manganese] or BCPM [$(CH_3C_5H_4)_2Mn$: bismethylcyclopentadienyl manganese] [Migita, 1988]. Carbon and oxygen have been detected within the MOCVD-prepared films. Solid zinc, sulfur and manganese are the source materials for the MSD method. In the sputtering process, a mixture of ZnS and MnS powders is commonly used as the source target while the sputtering gas is argon. Hydrogen sulfide gas is sometimes added in the sputtering system to reduce the sulfur vacancy concentration. Argon contamination has been found in sputtered ZnS films. In HTCVD, ZnS and Mn powders are used as source materials while argon (or hydrogen) and hydrogen chloride are employed as the carrier gas. Chlorine has also been detected in these films.

HTCVD is attractive due to its capability of producing films with large crystal grains (as large as 60 nm), bright luminescence, and excellent aging stability [Mikami, 1992]. Additionally, HTCVD is potentially well suited to low-cost, large-area deposition.

At high temperature, around 900 °C, the ZnS source sublimates and is carried to the reaction chamber by a carrier gas (H_2 or Ar) . The chemical reaction is given by:

$$2\ ZnS\ (s) \rightarrow 2\ Zn\ (g) + S_2\ (g).$$

An activation energy of 92 Kcal/mol has been reported for this process [Mikami 1991]. On the other hand, Mn chemically reacts with HCl, as given by the following equation:

$$Mn\ (s) + 2HCl\ (g) \rightarrow MnCl_2\ (g) + H_2\ (g)\ .$$

All gas species impinge onto the substrate simultaneously. The growth process is shown schematically in Figure 2-3. The deposition process occurs as follows:

1. Reactants (Zn, S_2, H_2S, and $MnCl_2$) transport to the surface of the growing film.
2. The reactants absorb onto the film surface.
3. Zn diffuses along the surface until it finds a low energy site and is incorporated into the film. S_2 , $MnCl_2$, and H_2S must first dissociate.
4. For each Mn incorporated into the film, a product molecule, most likely $ZnCl_2$ desorbs.

During deposition, the growth rate depends strongly on the growth kinetics involved. Mikami et al. reported the dependence of growth rate on the substrate temperature. The growth rate increases initially with increasing substrate temperature and reaches to a maximum value at 550 °C. Below 500 °C, thin film growth is limited by surface-kinetic control (processes 2 and 3 above). Between 500 - 550 °C, the growth kinetic may shift from surface-kinetic to mass-transfer control (process 1 above). At higher temperature, the growth rate decreases sharply. This phenomenon may be due to fast desorption of the adsorbed reactant species or due to depletion from earlier reaction in the reactor.

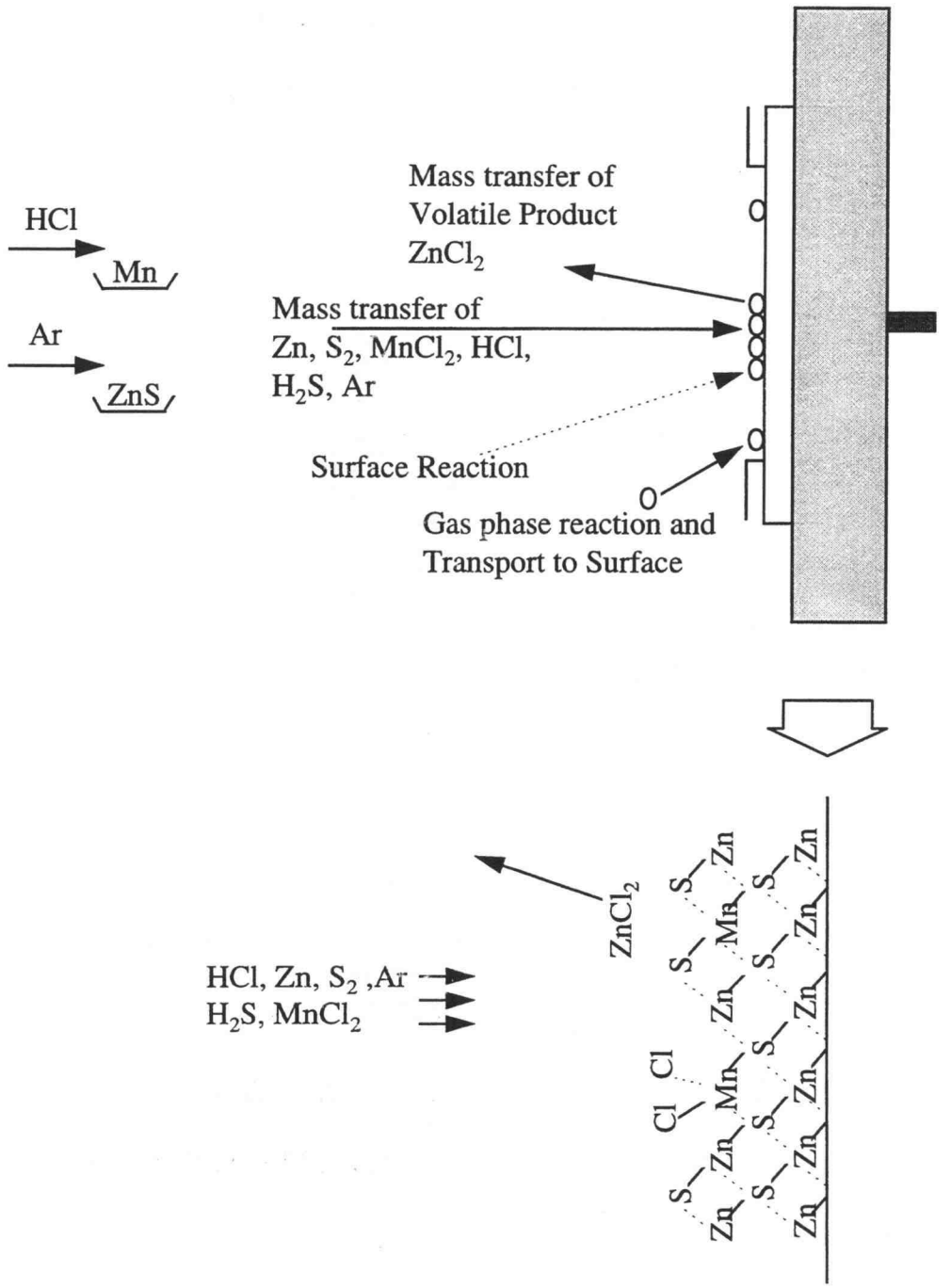

Figure 2-3. Deposition process in low pressure HTCVD system.

2.5 Structure and Chemical Characterization of ZnS:Mn Phosphors

ZnS:Mn thin films deposited for EL devices are polycrystalline films with strongly preferred orientation in the (111) direction for the cubic phase or the (002) direction for the hexagonal phase, regardless of the deposition process. The crystal phase formation of ZnS:Mn depends strongly on deposition methods and experimental conditions. For ZnS single crystals, the transition temperature from the cubic phase to the hexagonal phase is 1020 - 1150 °C at atmospheric pressure [Weast, 1990]. The hexagonal phase, however, may be formed at a lower temperature during reduced pressure deposition processes which may be far from thermodynamic equilibrium. ZnS thin films are predominantly cubic when deposited by PVD methods. When CVD methods are used, they are hexagonal. This may be due to the different substrate temperatures; 350 °C or lower for PVD methods and 400 - 600 °C temperature range for CVD methods [Ono, 1995]. In addition, other reactor parameters and dopant level can affect the crystal structure environment around the Mn site [Adachi, 1993; Kennedy, 1995].

The crystal size of ZnS varies with deposition method [Blackmore, 1991; Ono, 1995; Theis, 1983]. ALE produces the largest crystallites -- as large as 100 nm is obtained for film thickness of 500 nm. HTCVD, MOCVD, and EBE have average sizes of 60, 45, and 25 nm, respectivelv. Crystallite size affects EL device efficiency. Regardless of deposition method, most films exhibit nonuniform columnar or conical

growth with initially a fine grain and larger crystals on the top [Oikkonen, 1985; Theis: 1983, 1984; Tanninen, 1983].

Different types of microstructure such as polytypes, microstrain, microtwin, and dislocation density in ZnS films have been investigated [Tanninen 1982, 1983]. However, the dependence of crystallinity, orientation, structure, and microstructure on luminescent property is still poorly understood.

The chemical composition, stoichiometry and impurity content of ZnS:Mn films also have significant influence on the performance of EL displays. The dependence of brightness and emission efficiency on the luminescent center concentration has been well investigated [Cattell, 1983; Mach, 1984; Mikami, 1991; Sasakura, 1981]. The desired Mn concentration may be achieved by adjusting the amount of source materials, substrate temperature, or source material temperature. Different atomic ratios of Zn to S have been reported for different process techniques and at different Mn dopant levels [Banovec, 1990; Mikami, 1992; Xian, 1994]. The chemical composition of ZnS:Mn films at different depths has been studied by using Auger electron spectroscopy (AES) [Banovec, 1990; Higuchi, 1988]. Higuchi reported that the effect of annealing on the structure yield a change in chemical composition distribution. In this research, a reduction of crystal defects was observed after the film was annealed. However, Mn, surprisingly, segregated to insulator phosphor layer interface instead of being more uniform distribution with annealing. Further studies of annealing effects on impurity migration are necessary.

Many techniques have been applied to determine the structure and chemistry of ZnS:Mn thin films. Among them, x-ray diffraction (XRD) and reflection high-energy

electron diffraction (RHEED) have been used to analyze crystal phase, preferred orientation, microstructure, thickness, and lattice constant. With transmission electron microscopy (TEM), the cross-sectional image of columnar growth and distribution of crystal size can be visualized. Surface topography of ZnS:Mn is viewed by scanning electron microscopy (SEM). Electron spin resonance (ESR) can determine the local Mn crystal environment. Other analytical tools, like electron microanalysis (EM), secondary ion mass spectrometry (SIMS), Auger electron spectroscopy (AES) and Rutherford backscattering spectroscopy (RBS) are often used to determine the Mn concentration, the ratio of Zn to S, impurities, and concentration vs. depth.

2.6 Luminescent Properties of ZnS:Mn Phosphors

Mn^{2+} ions play the role of luminescent center when doped into ZnS host lattice. The photo- and electroluminescent emission of ZnS:Mn thin films show a yellow-orange emission with a maximum peak at approximately 585 nm [Falcony, 1992; Migita, 1988; Mikami, 1991; Ono, 1995; Ouyang 1989], suggesting the radiative relaxation transition of 3d electrons of Mn^{2+} center from the first excited state, $^4T_1(G)$, to the ground state, $^6A_1(S)$ [Pohl: 1993: 1989].

It is well known that the luminescent intensity of Mn-doped ZnS increases with Mn concentration up to an optimum concentration (about 0.5 to 1 at. %), indicating that more Mn activators are available for impact excitation followed by radiative relaxation. The intensity, however, decreases dramatically and is accompanied by a red emission

shift at higher Mn concentrations [Cattell, 1983; Mach, 1984; Mikami 1991, Sasakura 1981]. It has been shown non-radiative relaxation between Mn pairs leads to luminescent quenching. It has been proposed that Mn clusters or MnS microphases lead to red emission [Bhise, 1990; Li, 1988; Nandagawe, 1991; Thong 1984].

The luminescent characteristics of ZnS:Mn is also affected by defects including: impurities coming from the precursors employed or reactor contamination, vacancies (anions or cations), and the change of crystal environment. Contaminants such as chlorine [Mikami 1991], copper [Mikami 1991], carbon [Migita 1988, Tammenmaa 1987], oxygen [Migita 1988, Lindroos 1995], and argon [Xian 1994] have been found in ZnS:Mn films grown by different deposition methods. These impurities may contribute to a different luminescent mechanism, peak shift, or a decrease or increase of luminescence efficiency. Migita et al. reported the decrease of PL intensity of ZnS:Mn caused by carbon and oxygen contamination. Different satellite emissions, such as blue [Mikami, 1991], green [Georgobiani, 1991; Mikami 1991], and red color caused by defects have been reported. Photoluminescence of undoped ZnS has also been studied to investigate the effect of different vacancy types and their levels on ZnS [McClean, 1992]. In order to evaluate the characteristics of activators and defects in ZnS films, luminescence has been examined at lower temperatures (from 12 - 273 K) [Thomas, 1989; Oda, 1979; Era, 1968]. At lower temperatures, PL properties, such as intensity, peak shift, and zero phonon line are investigated. Thomas and his coworkers [McClean, 1992; Thomas, 1989] reported a change of PL intensity and peak shift of ZnS:Mn and undoped ZnS samples after annealing.

Photoluminescence (PL) and electroluminescence (EL) measurement of ZnS:Mn thin films have been extensively investigated. However, only one study reporting the relationship of PL and EL emission has been found [Zhang, 1989]. Due to the different excitation processes and energy transfer mechanisms, the intensities are different, and the peak broadens between PL and EL.

The stability of the EL device is crucial in developing EL displays for the market place. Aging studies have been investigated by brightness-voltage (B-V) technique [Inoguchi, 1974; Mikami 1992]. During the aging process, two types of aging phenomena are generally observed: the positive shift (P shift) and negative shift (N shift). In the P shift, the threshold voltage increases during aging. The N shift is in the opposite direction. Both aging patterns have been addressed in the literature. ALE films show N shifts, while evaporated film shows P shift. Mikami et al. [1992] have demonstrated that the growth temperature is the key parameter in determining N shift or P shift of HTCVD films. Finally, they also present a long life stable ZnS:Mn EL device in which the phosphor is prepared by HTCVD. Nevertheless, the mechanism for the curve shift and/or softening is not fully understood.

2.7 ACTFEL Device Electrical Characterization

In addition to understanding the influence of structure and chemical properties on emission in ZnS:Mn, knowledge of the physical phenomena governing electroluminescence is useful in engineering high performance ACTFEL displays. Physical models and electrical characterization techniques have been proposed by several authors in order to better explain the mechanism of electron transport, excitation and relaxation in the phosphor under an applied electric field. The internal charge and field strength model for EL devices was first proposed by Bringuier [1989] to examine internal charge behavior. The model described the relationship of internal charge with the applied voltage and capacitance of the phosphor and insulator. Based on the charge versus voltage (Q-V) technique and Bringuier's model, Wager and his co-workers [Abu-Dayah, 1993] developed the charge versus phosphor field ($Q\text{-}F_p$) technique to interpret charge transport phenomenon during the rising positive and negative voltage pulse. Internal electrical characteristics, such as conduction charge (Q_{cond}), polarization charge (Q_{pol}), and leakage charge (Q_{leak}) have been assessed. With the addition of the capacitance versus voltage (C-V) technique proposed by McArthur [1990], the existence of space charge generation in the phosphor layer has also been studied, through the C-V overshoot deviation and the lack of field clamping in $Q\text{-}F_p$ curve [S. Shih, 1995, 1996]. Moreover, aging can be studied by C-V and $Q\text{-}F_p$ techniques. Abu-Dayah [1994] has reported the interface asymmetrical aging studies of ALE ZnS:Mn.

Chapter 3

Experimental Techniques

3.1 Halide Transport Chemical Vapor Deposition System

Undoped ZnS thin films, as well as ZnS:Mn and ZnS:Cl, were deposited by low pressure halide transport chemical vapor deposition. A schematic of the deposition system is shown in Figure 3-1. The HTCVD reactor consists of modular graphite subunits (reaction chamber, substrate holder and, source heaters) within a stainless steel pressure barrier. This assembly is housed within a three-zone horizontal furnace. The substrate holder is positioned normal to the gas flow. Two internal graphite heaters provide additional heating to the Mn (ESPI, 99.997%) and ZnS (ESPI 99.99%) source materials. High purity HCl (ESPI, 99.997%) gas flows through the Mn heater while H_2S (Air product, 99.9995%) and Ar (Air product, 99.9995%) flow through the ZnS heater. These gases are piped through a mass flow controlled manifold into the reaction chamber. The pumping system, which is located in a pump room beneath the reactor, consists of a roots blower, backed by a mechanical pump. Temperature is monitored and controlled separately at the substrate and in each of the source heaters. Pressure in measured using a capacitance manometer. A load lock facilitates loading and unloading of samples.

The source heaters were modified from the original design [Miller, 1995] to improve their reliability. A side view and a cross sectional view of the heaters are shown in Figures 3-2 and 3-3 respectively. The heating wire is wrapped in nineteen, three inch

long ceramic (99.8% alumina) tubes placed around the graphite heaters. The tubes are then secured with electrically insulating cement. Repeated failure of the nichrome ZnS heater wire at high temperature was overcome by switching to molybdenum wire. Temperature is set using a variable resistance Variac.

A detailed experimental protocol for film deposition is described in Appendix A. The system pressure is kept lower than 0.2 torr. The ranges of process parameters which are studied are listed in Table 3-1. These parameters include: ZnS source temperature, Mn source temperature, argon, hydrogen chloride and hydrogen sulfide gas flow rates, and deposition time. The characteristics of the deposited films depend on the substrate on which they are grown. Substrates, include bare 7059 corning glass substrates, ATO [(ATO/glass) or (ATO/ITO/glass)], and ALE grown ZnS (undoped ZnS/ATO/ITO/glass).

Table 3-1. Reactor Conditions for HTCVD Growth of ZnS:Mn and ZnS:Cl Films.

	ZnS:Mn	ZnS:Cl
Substrate temperature	470 - 600 °C	550 °C
ZnS Source temperature	850 - 1020 °C	900 °C
Mn source temperature	600 - 775 °C	
Total pressure	< 0.2 Torr	< 0.2 Torr
Gas flow rates: Ar	0 - 100 sccm	40 sccm
H_2S	0 - 0.4 sccm	
HCl	0 - 3 sccm	1.0 sccm

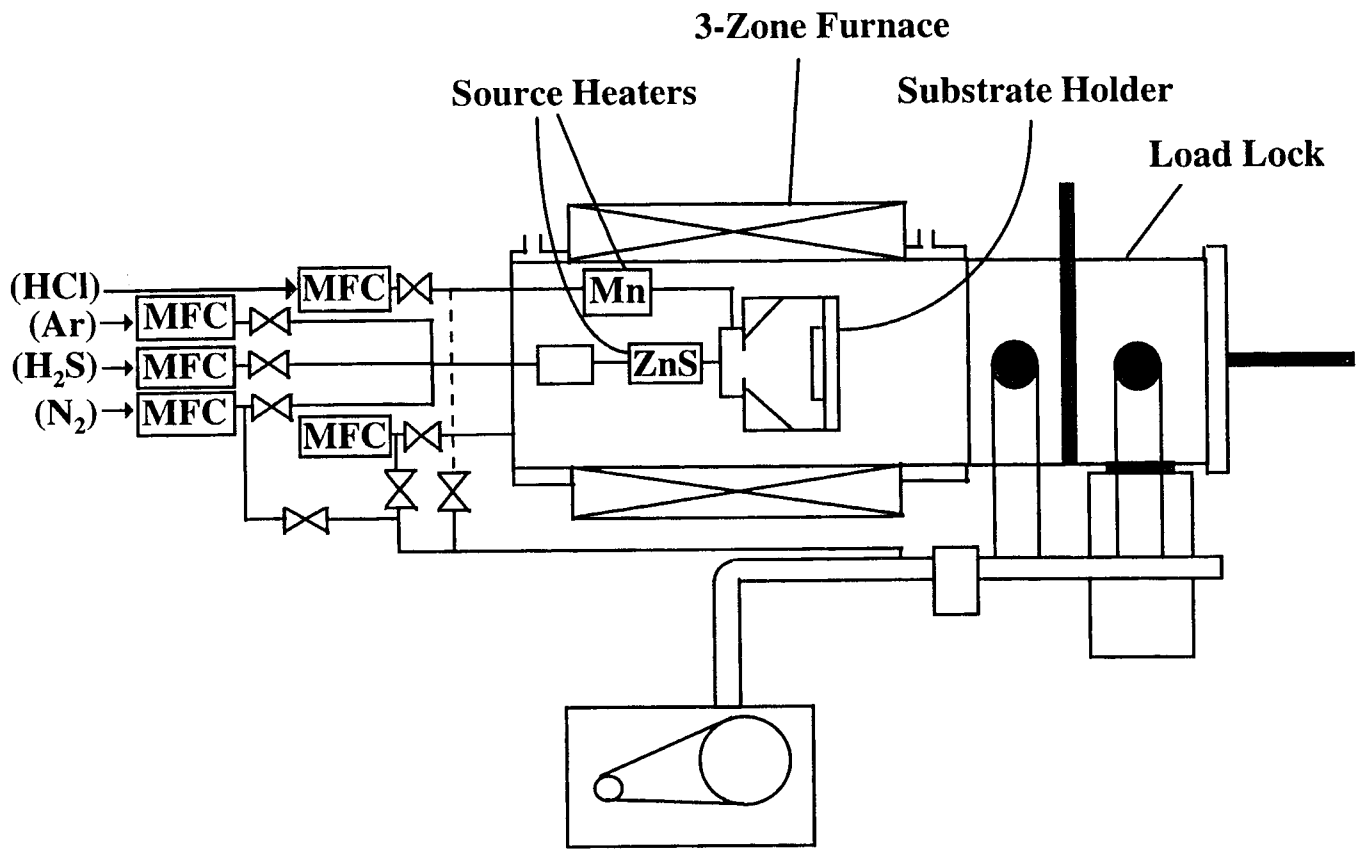

Figure 3-1 Schematic diagram of the halide transport chemical vapor deposition reactor

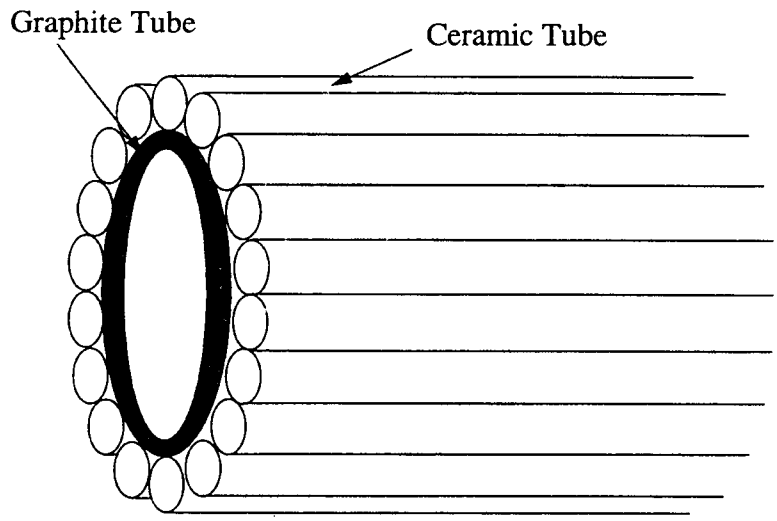

Figure 3-2 Side view of the ZnS and Mn source heaters

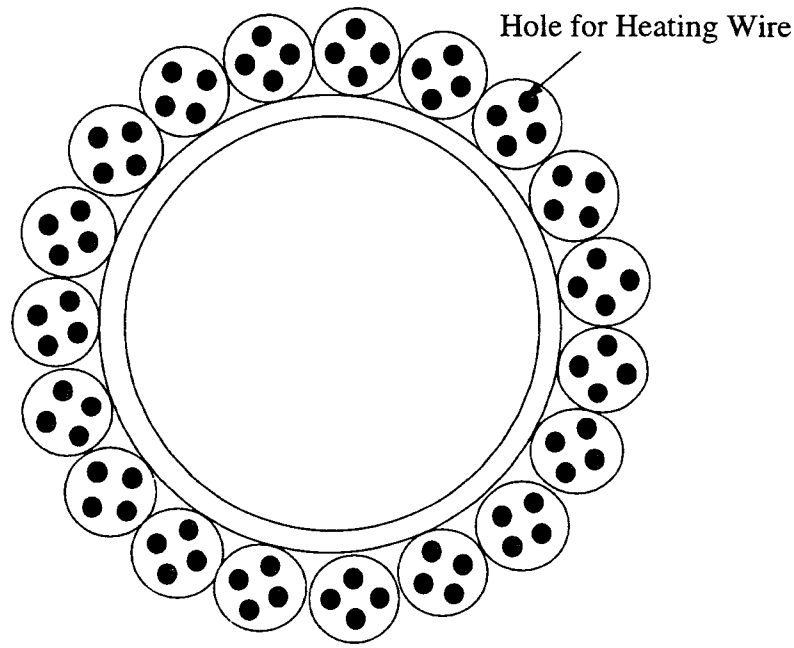

Figure 3-3 Cross section of the ZnS and Mn heaters

3.2 Insulating and Conducting Layer Fabrication for ACTFEL Devices

The insulating films used to prepare EL devices consist of ATO and silicon oxynitride. ATO films of about 2500 Å thickness were grown by Planar Systems, Inc. The SiON insulating layer with a thickness of about 2000 Å is fabricated by plasma enhanced chemical vapor deposition (PECVD) using a parallel plate rf (13.6 MHz) plasma. 75 W of power and a pressure of 0.5 torr are used. In order to obtain films with a refractive index of 1.6, the flow rate of SiH_4, N_2O and N_2 gas are 10, 75, and 100 sccm, respectively. The substrate temperature is 300 °C and the deposition time is 12 minutes.

A transparent ITO layer, fabricated by Planar Systems, Inc., is used for the bottom electrode. The thickness of ITO is approximately 2000 Å. The top electrode is made of aluminum and is deposited by thermal evaporation with a thickness of 1500 Å

3.3 Structural and Chemical Analysis

The crystallinity analysis of the ZnS thin films is performed at room temperature by x-ray diffraction (XRD) using a Siemens D5000 diffractometer with Cu Kα radiation. The two-theta scanning range is between 2° and 90° with a θ step width of 0.02°. The crystal phase (cubic or hexagonal), the lattice constant, the preferred orientation and the crystal size can be accessed from XRD data. Cross-sectional images of a ZnS:Mn sample are obtained by transmission electron microscopy (XTEM) micrographs using a

magnification of 100,000x. Film thicknesses are measured using ellipsometry and profilometry.

The bulk chemical composition of ZnS:Mn films are determined by electron microprobe. The electron beam accelerating voltages is 7 keV. Fluorescence x-rays, where frequency is characteristic of a given elements, are detected. Surface chemical analysis is done by Auger electron spectroscopy with a 3 keV electron beam source. Ion beam sputtering allows depth profiling to a resolution of 20 Å, so the chemical composition very close to the surface can be accessed. Electron energy ranges from 0 to 1000 eV and transitions of KLL and LMM type Auger electrons are detected.

The local crystal environment of Mn luminescent centers are analyzed by electron spin resonance (ESR). The spectra are obtained using a Bruker ESP 300 X-band spectrometer. The modulation frequency is 100 kHz and the modulation amplitude is 3.88 Gauss.

3.4 Optical Characterization Techniques: Photoluminescence (PL), Electroluminescence (EL), and Decay time

Photoluminescence (PL) of ZnS:Mn and ZnS:Cl thin films are measured using a computer-controlled right angle spectrometer. An Oriel 300-W Xe lamp is used as the excitation source. The source light is passed through a 50-cm water filter and filtered first with a prism monochromator, and then onto the sample. The PL is collected at a right angle to the excitation, dispersed through a monochromator, and detected with a

Hamamatsu R636 photomultiplier tube. The signal is collected and amplified with a Keithley model 602 picoammeter and then converted to a digital signal for computer acquisition. PL of ZnS:Cl is measured at room temperature and 12K.

A bipolar pulse of trapezoidal shape with a 5 μs rise/fall time, pulse width of 30 μs, and a frequency of 1 kHz is used for electroluminescence (EL). The brightness is measured vs. the driving voltage of this pulse. The luminescence decay of excited centers is also measured.

3.5 Internal Charge-Phosphor Field (Q-F_p) Technique

The Q-F_p method measures the internal electrical characteristics of the phosphor, such as the conduction charge, relaxation charge, leakage charge, polarization charge, and the steady-state electric field. This technique has been developed by Wager and co-workers as mentioned in Chapter 2. A Sawyer-Tower configuration is used, as shown in Fig. 3-4.

A bipolar pulse of trapezoidal shape with a 5 μs rise/fall time, pulse width of 30 μs, and a frequency of 1 kHz is used. This waveform drives a resistor (200Ω), the ACTFEL device, and a sense capacitor (10 nF) is connected in series. By monitoring the temporal response of the voltage before and after the ACTFEL device and applying the appropriate circuit analysis, the internal charge, Q, and the phosphor field, F_p, is determined. Q-F_p curves are then generated for a given peak voltage of the driving waveform.

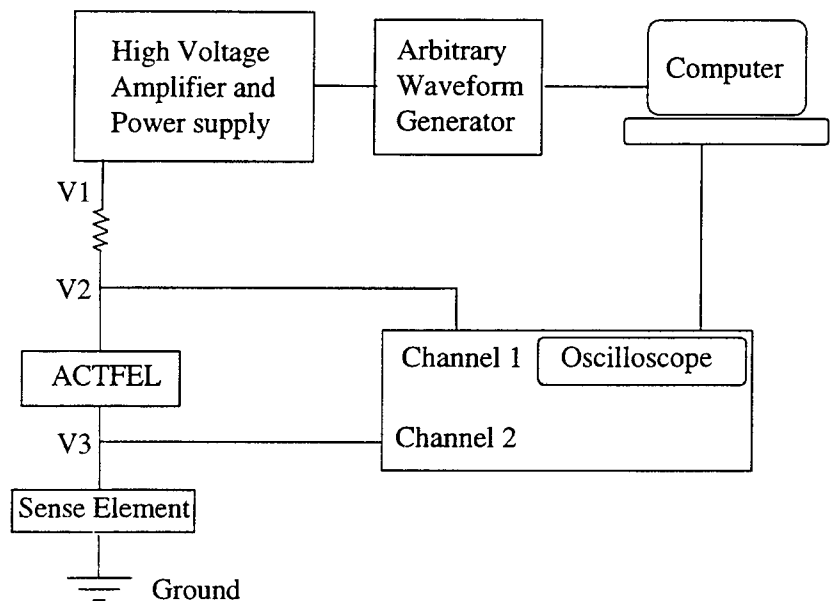

Figure 3-4. Sawyer-Tower configuration for electrical characterization

Chapter 4

Growth, Structural and Chemical Characteristics of ZnS:Mn Phosphors

Reported literature of ZnS:Mn thin films for ACTFEL devices have always demonstrated a strong preferred orientation with a XRD peak at $2\theta = 28.6^{\circ}$, regardless of process methods, experimental conditions, or crystal phase (hexagonal or cubic). Moreover, different deposition methods usually produce either hexagonal or cubic films, regardless of experimental conditions. For example, ALE produces hexagonal films while e-beam evaporation produces cubic films. Using HTCVD, we can control the crystal phase of ZnS:Mn thin film under different processing conditions. When pure argon is used as a carrier gas, a strong preferred orientation at 28.6° is obtained consistent with earlier reports. This film has a hexagonal structure. With the addition of H_2S gas to the our system, however, growth at 56.4° becomes dominant. Meanwhile, the crystal structure changes from hexagonal to cubic. By modifying the source temperature and substrate temperature, the degree of preferred orientation can be altered. The effect of H_2S gas on crystal orientation and structure will be discussed in Chapter 6. This chapter will focus on the change of XRD peak intensity under different processing conditions, the properties of undoped ZnS thin film, and effect of substrate on structure.

4.1 Growth Characteristics of ZnS:Mn Thin Films

Control of growth rate, crystallinity, composition and texture of ZnS:Mn thin films are important issues in preparing ACTFEL displays. Therefore, the growth characteristics, such as the transport rate of source material, the effect of carrier gas flow rate on film growth, and effect of the substrate on the crystal structure of growth film are investigated.

Figure 4-1 shows the dependence of the transport rate of ZnS source material on temperature. The carrier gas consists of 0.4 sccm H_2S and 39.6 sccm Ar. The transport rate is calculated from weight difference of ZnS source material. A logarithmic relationship relates the source temperature and transport rate. A ZnS source temperature higher than 850 °C is necessary to obtain sufficient vapor pressure. No detectable ZnS film is seen on the substrate when a source temperature below 850 °C is used. The transport process is associated with the dissociation of ZnS source material, according to the following reaction:

$$2ZnS(s) \Leftrightarrow 2Zn(g) + S_2(g) .$$

Figure 4-2 shows the results of ZnS transport rate as a function of carrier gas flow rate. The ZnS source temperature is fixed at 980 °C throughout the experiment. The transport rate is linear with flow rate up to 60 sccm, but levels off at higher flow rates. The source material is carried by argon gas into the reaction chamber, causing ZnS weight loss. At low flow rates, transport is limited by how quickly the carrier gas can sweep away the sublimated Zn and S_2 species; thus a linear relation between flow and transport

results. At higher flow rates, the sublimation of solid ZnS limits transport, causing the curve to level off. This limit is exponential in temperature. We predict, therefore, that the lower the source temperature the earlier the transport rate levels off with flow rate.

XRD is employed to examine the crystal quality of ZnS thin films as well as characterize the growth process. XRD patterns of ZnS:Mn thin films grown for 1, 2, 3 hours are shown in Figure 4-3. The source temperatures of ZnS and Mn are fixed at 940 °C and 725 °C, respectively. Flow rates of 39.6 sccm argon and 0.4 sccm hydrogen sulfide are passed through the ZnS heater. Hydrogen chloride flow rate through the MnS heater varies between 0.6 - 0.8 sccm. The XRD peak intensity increases with deposition time. Figure 4-4 plots the sum of the two dominant peaks' (2θ = 28.6° and 56.3°) integrated intensity vs deposition time. Assuming the film thickness is proportional to deposition time, the integrated intensity of the XRD peak is linear with thickness. This result has been reported previously [Blackmore, 1991], and suggests that the x-ray diffraction may be used to estimate film thickness.

Next, the XRD spectra at carrier flow rates of 40, 60 and 100 sccm, shown in Figure 4-5, are compared. The substrate temperature is 550 °C. The peak intensities are approximately independent of flow rate from 40 to 100 sccm. However, recall the ZnS transport rate is enhanced from 3.2E-4 to 5.9E-8 mole/min (Figure 4-2). This result indicates that at 550 °C, the reaction rate is surface controlled even at flow rates as low as 40 sccm. Hence, flow rates around 40 sccm are used in this thesis.

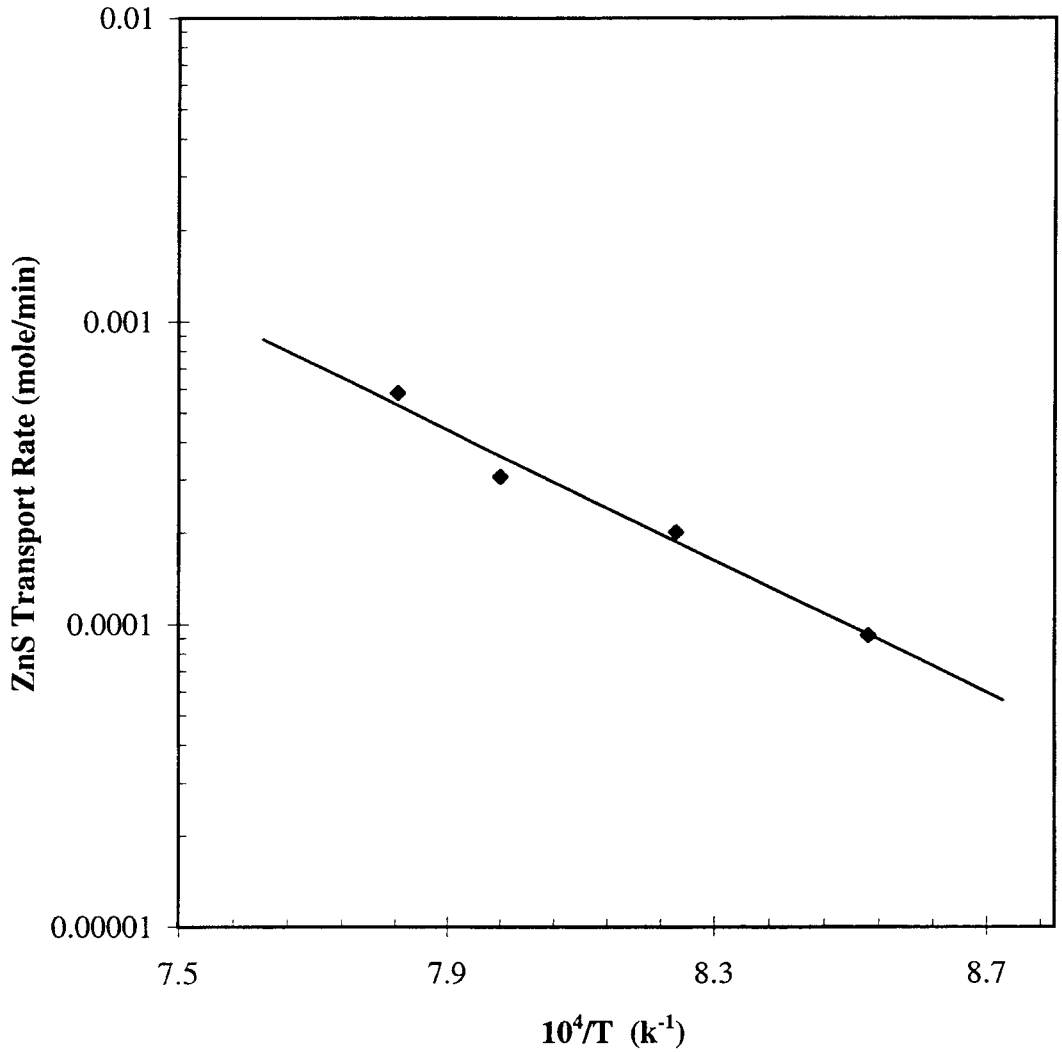

Figure 4-1. The dependence of ZnS transport rate of source temperature.

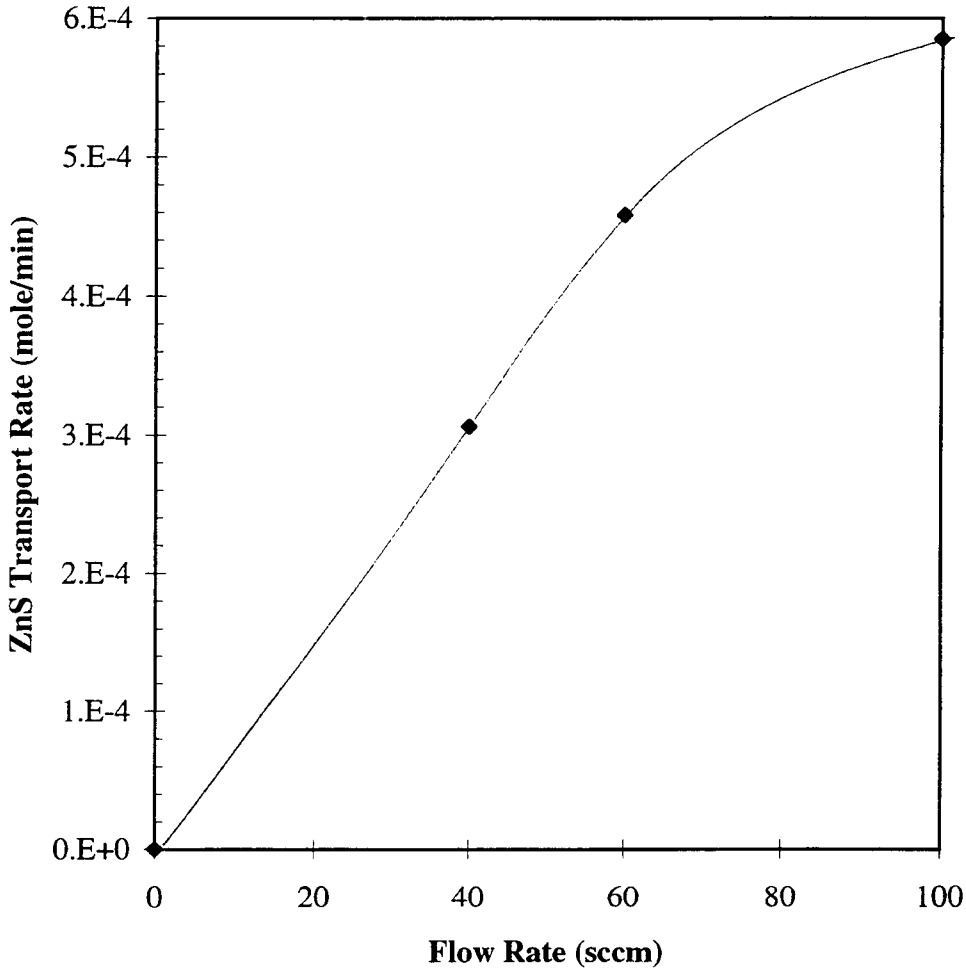

Figure 4-2. The effect of 1% H_2S/Ar gas flow rate on ZnS transport rate. The ZnS source temperature is fixed at 980 °C.

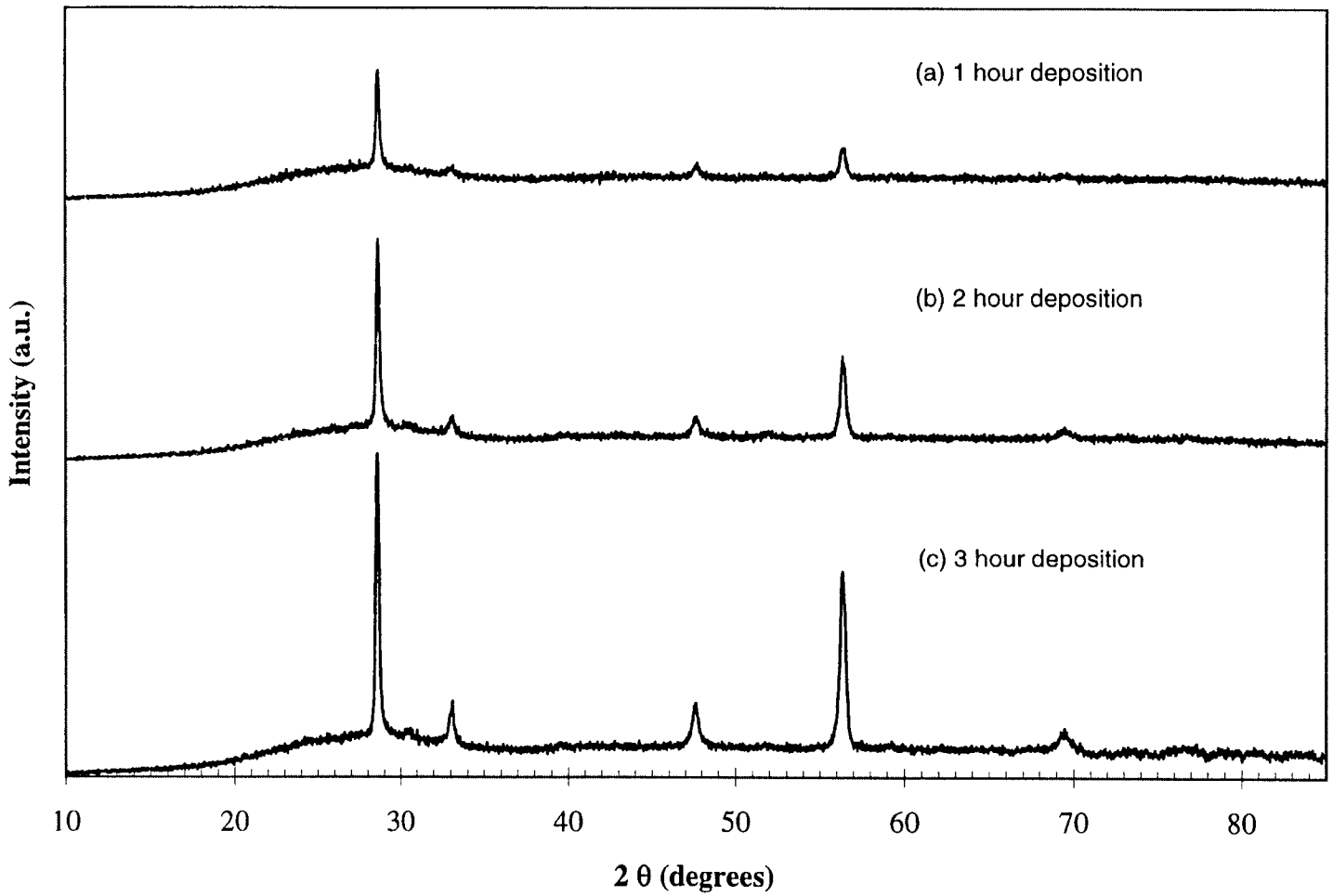

Figure 4-3. XRD of ZnS:Mn thin film grown with different deposition times.

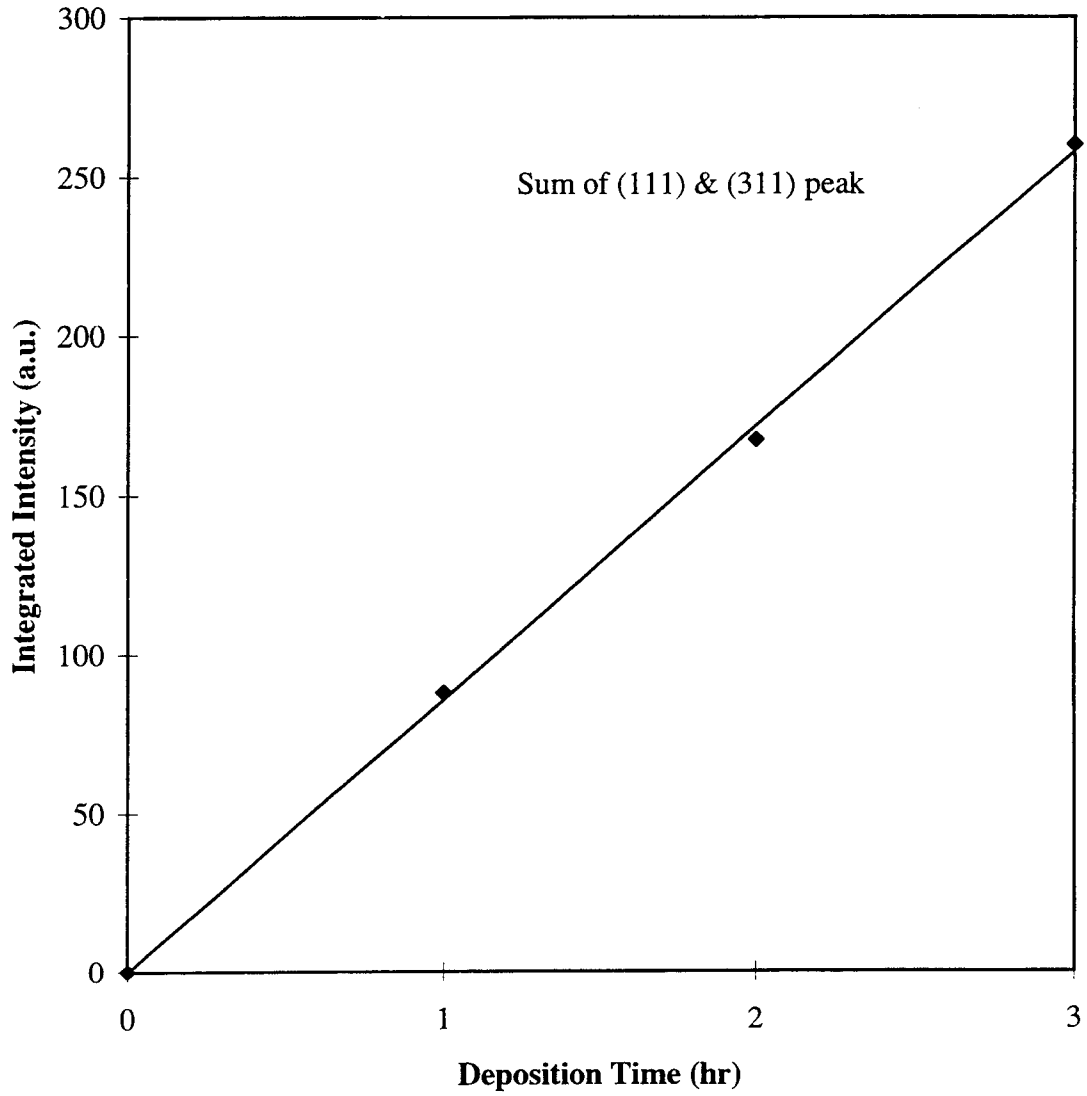

Figure 4-4. Integrated intensity of XRD peaks of ZnS vs deposition time

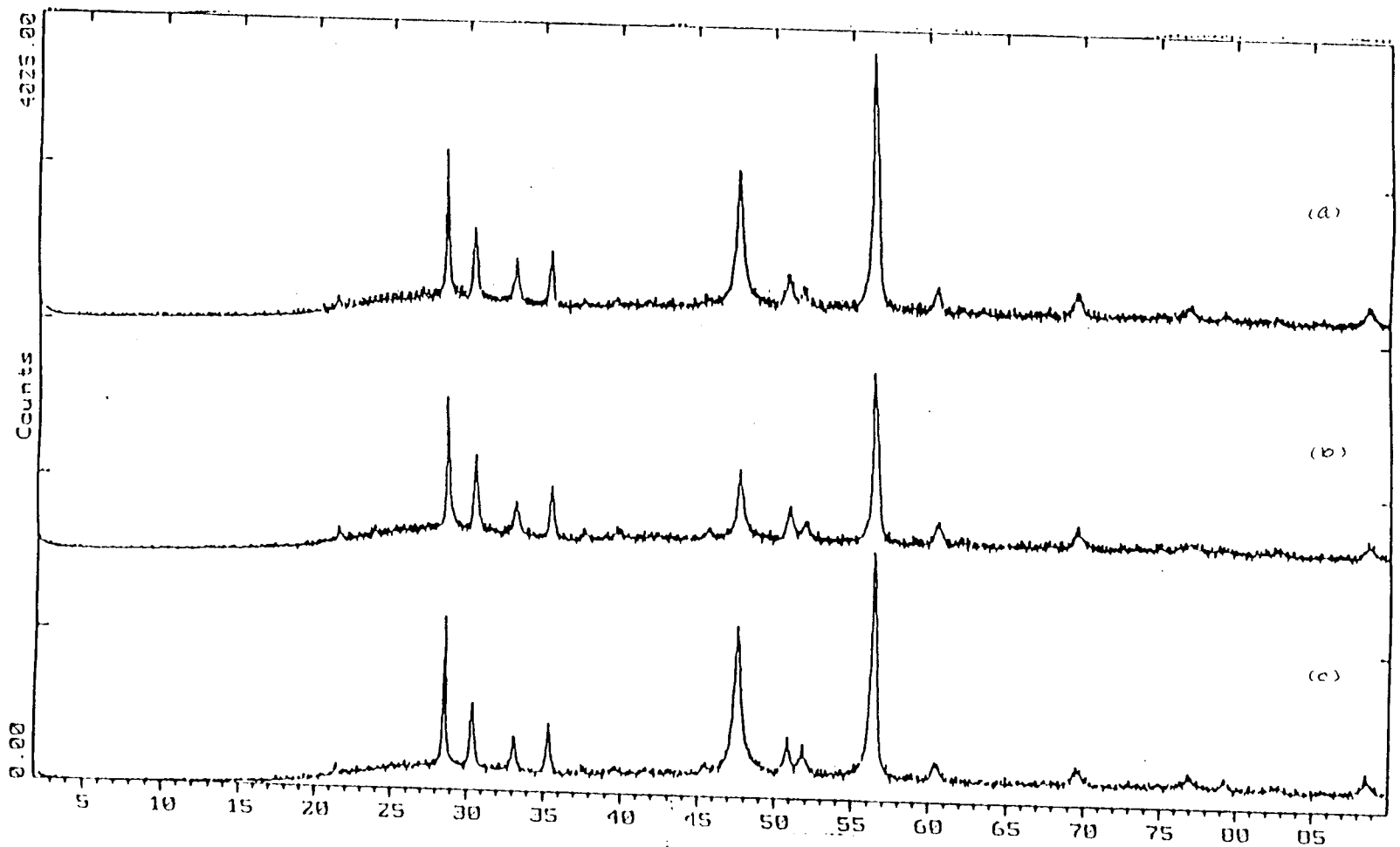

Figure 4-5. XRD: Dependence of crystal growth on 1%H2S/Ar gas flow rate
(a) 40 sccm, (b) 60 sccm, (c) 100 sccm

4.1.1 Structure of Undoped ZnS and ZnS:Mn Phosphors

At atmospheric pressure, the hexagonal structure of the ZnS crystal is thermodynamically stable at temperatures higher than the phase transition point of 1020-1150 °C. However, the formation of the ZnS hexagonal phase can be promoted by thin film processing conditions, such as: pressure, substrate temperature, and dopant. It is unclear whether this phenomena is based on energetics or kinetics; however the hexagonal phase of ZnS:Mn thin films has been reported at growth temperatures as low as 425 °C in low pressure systems [Ono, 1995]. In our study, the lowest substrate temperature used is 470 °C. ZnS:Mn films deposited at this temperature are hexagonal (see Chapter 5, Figure 5-1). In order to check the effect of the existence of manganese impurities (or HCl carrier gas) or the crystal structure, undoped ZnS thin films have been deposited. XRD spectra, presented in Figure 4-6 (a), show that even when substrate temperature is as high as 550 °C, the structure is still cubic. The hexagonal phase cannot be seen until the substrate temperature increases to 600 °C. In these spectra, the hexagonal phase is identified by peaks at $2\theta = 30.5^{\circ}$ and 51.7°, which correspond to (101) and (103) planes, respectively, shown in Figure 4-6 (b). Diffraction patterns of cubic films do not exhibit these peaks.

Cross-sectional images of ZnS:Mn thin films obtained by TEM are shown in Figures 4-7(a) and (b). These photographs are at 100,000X. The white region between the two films is epoxy that is used to prepare the cross section. The film surfaces show roughness on a scale of about 50 nm, with a film thickness of 450 nm. The surface

roughness ($\Delta t/t$) of this film is around 11%, which is smaller than ALE and EBE films [Theis, 1983]. Grains are smaller at the film interface and larger at the growth surface, and exhibit an average size of 100-200 nm. After building a device, the EL performance is investigated. The decay emission vs. time is shown in Figure 4-8. The brightness and decay times are not symmetrical for the positive and negative excitation pulses. During a positive pulse, electrons travel from the substrate (ITO/ATO) toward the growth surface. In this case, they are directed toward the larger grains. Since the electrons which were accelerated by the applied field need to travel a distance before they had enough energy to excite a luminescent center, the phosphor closest to the injection interface was not excited. During a positive pulse, the Mn in the larger grains was excited. On the other hand, during a negative pulse, the smaller grains became more dominant in their contribution to the luminescence. This non-symmetric morphology of the ZnS:Mn thin film as obtained from the TEM image seems to provide an explanation for this non-symmetric brightness and decay time measurement.

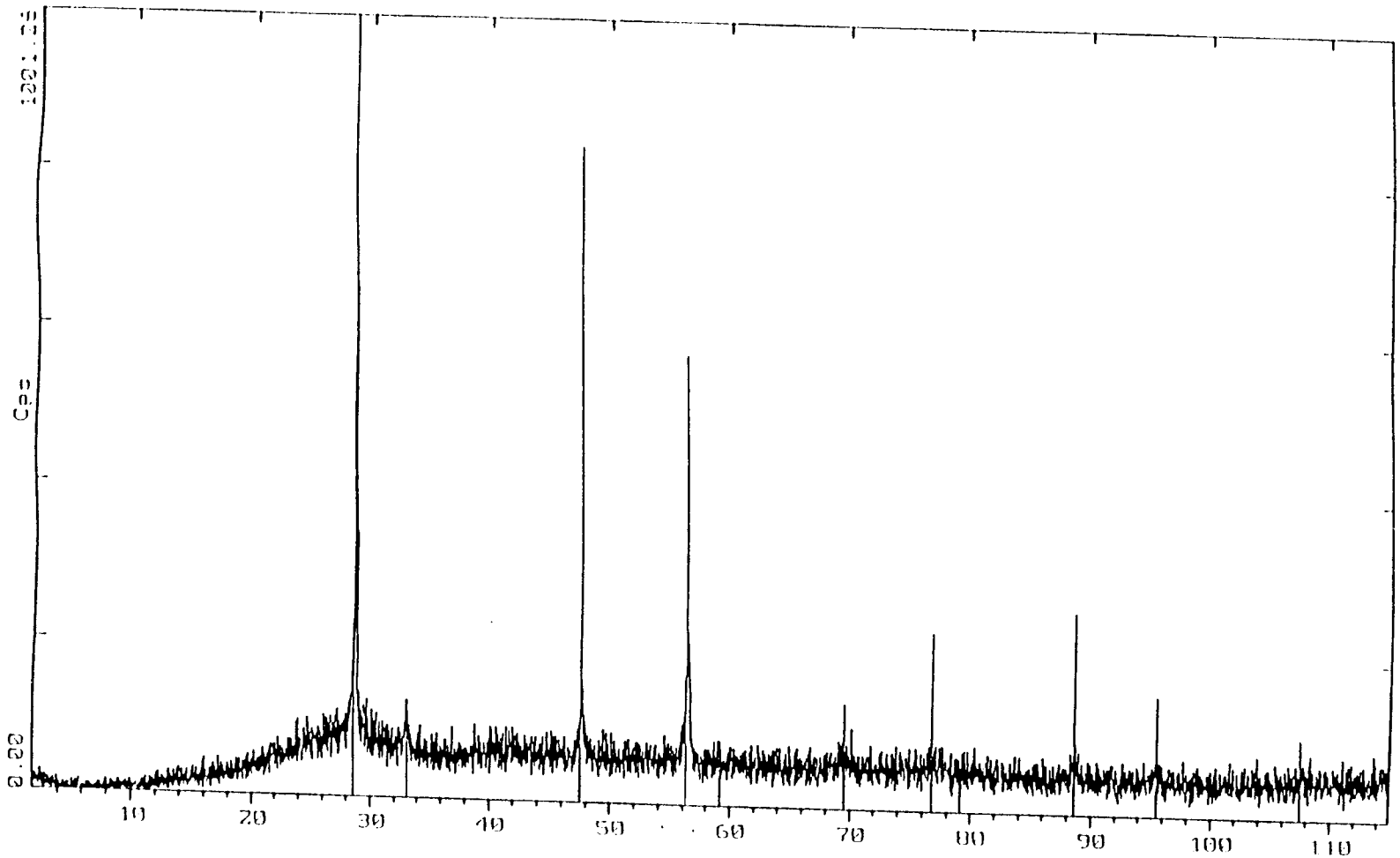

Figure 4-6(a). Undoped ZnS thin film deposited at 550°C

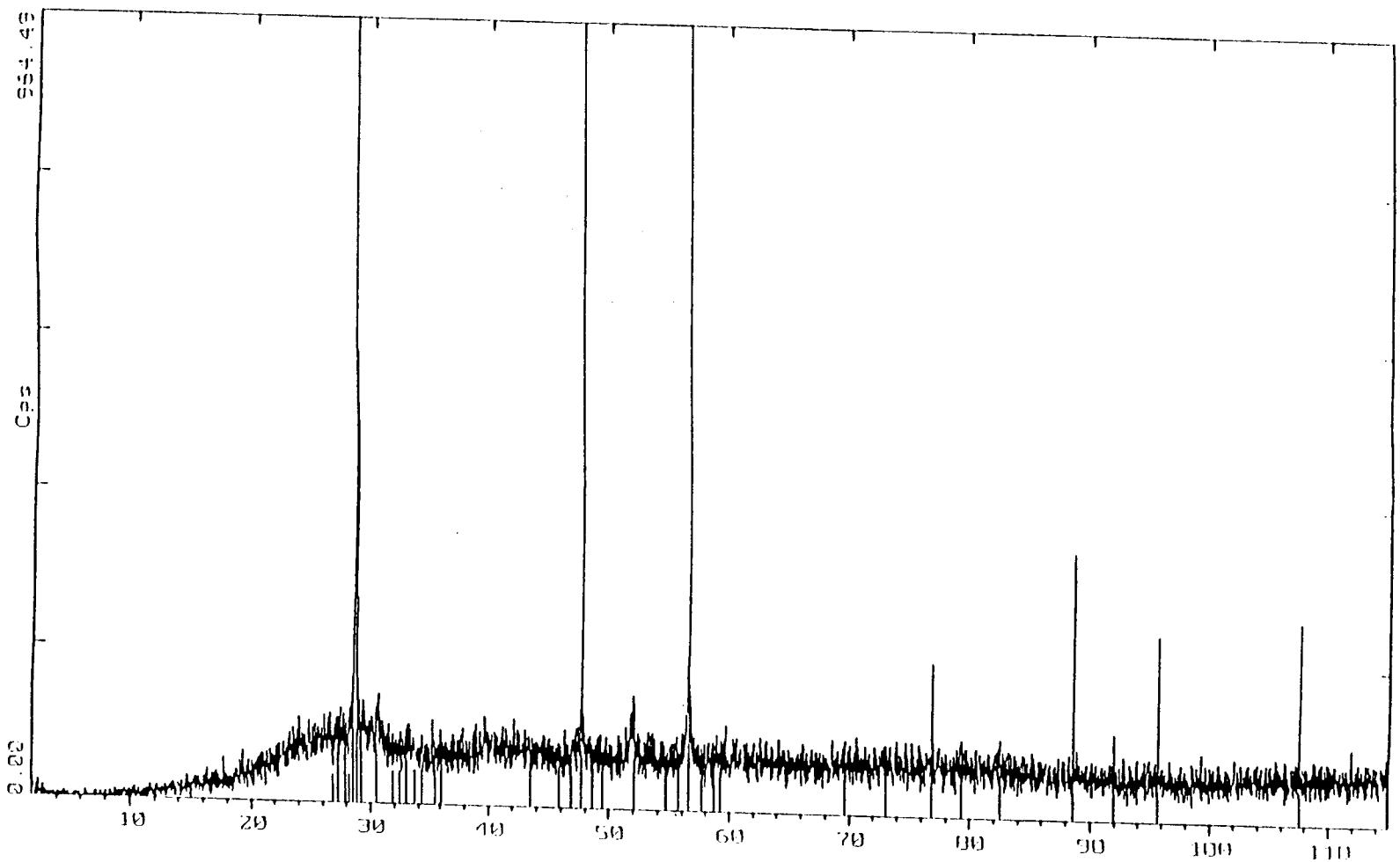

Figure 4-6(b). Undoped ZnS thin film deposited at 600°C

Figure 4-7(a). TEM cross-sectional image of ZnS:Mn thin film.

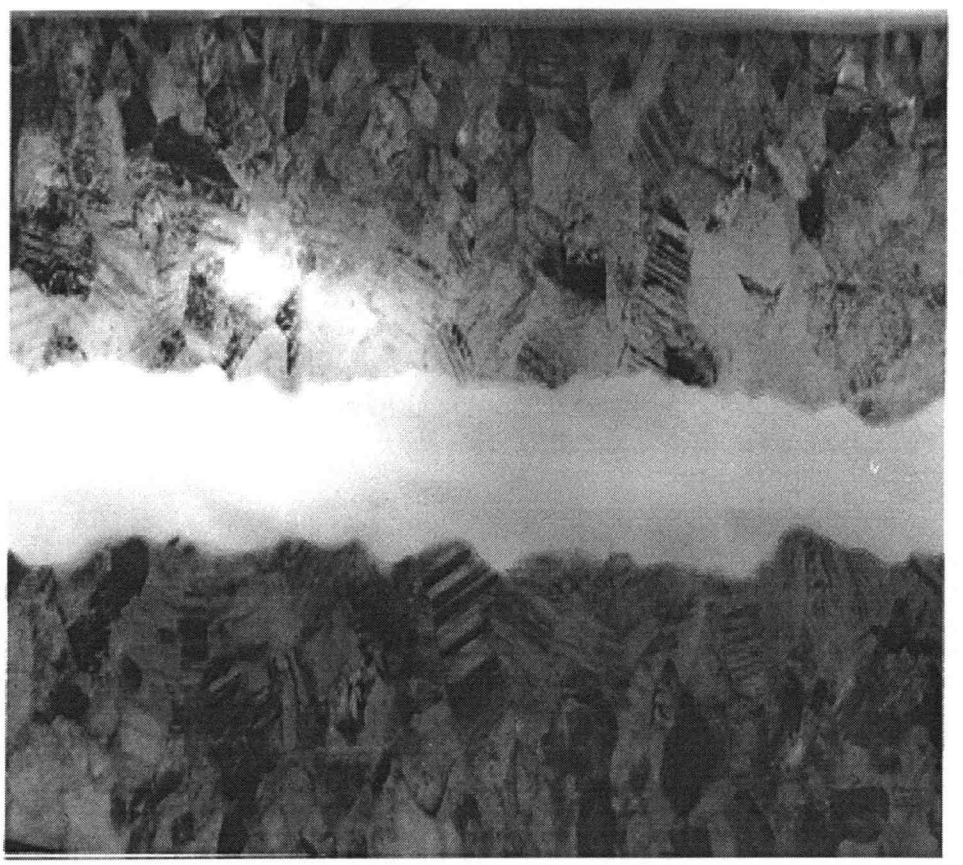

Figure 4-7(b). TEM cross-sectional image of ZnS:Mn thin film.

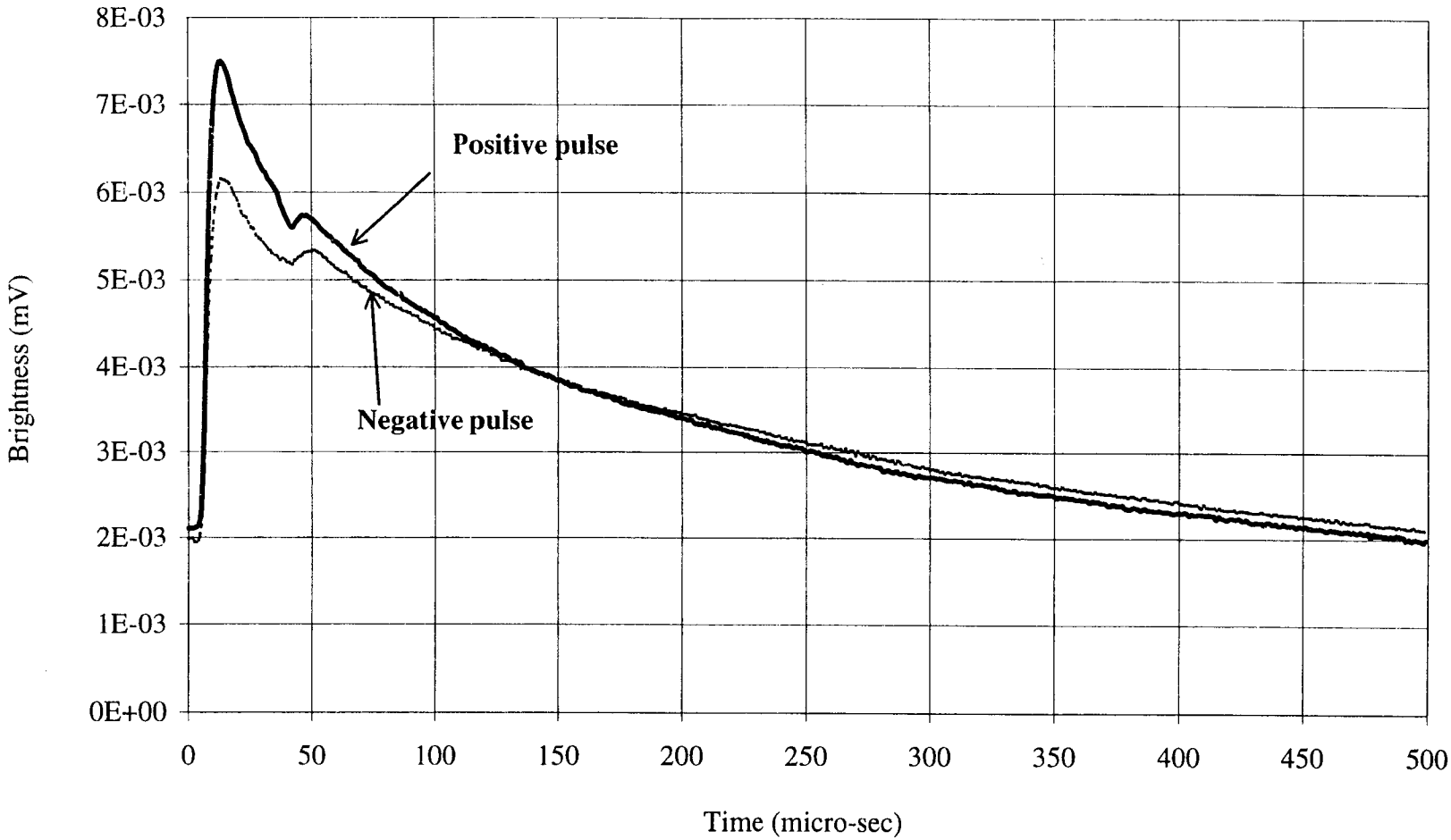

Figure 4-8. Decay time of HTCVD ZnS:Mn EL device.

4.1.2 The Effects of Substrate on ZnS:Mn Growth

The crystal phase and/or orientation may depend on the substrates on which the ZnS is grown. Blackmore et al. [Blackmore, 1991] reported that the (111) peaks of ZnS were broader and less intense on cadmium stannate (CS) than on glass due to the possible reaction between ZnS and Cd_2SnO_4 and the exchange of Zn-Cd across the ZnS-CS interface. They also demonstrated that the intensity and grain size of ZnS which is deposited on ZnO substrates depend on the (002) intensity and/or grain size of the ZnO substrate.

Mn doped ZnS films grown on the top of an amorphous ATO layer and bare glass have been compared. The (002) intensity and FWHM value are about the same, indicating the growth mechanism is similar on both amorphous substrates. A crystalline ITO layer below the ATO layer shows no effect as well. However, crystalline substrates have different effects. Cubic ZnS:Mn films deposited on substrates with and without thin hexagonal ZnS film (200 Å) were examined. This thin ZnS film was pre-deposited by Planar Systems using ALE. Before ZnS:Mn deposition by HTCVD, the 200 Å/ATO/ITO/glass was scanned by XRD and showed no detectable ZnS peak. The XRD patterns of the two films after deposition are shown in Figure 4-9. The film shown in Figure 4-9(a) is deposited on ATO/ITO/glass; another in Figure 4-9(b) is deposited on 200 Å ZnS/ATO/ITO/glass. Both films show similar patterns, except the appearance of a peak at $2\theta = 51.8^{\circ}$ in Fig. 4-9(b), indicates that the hexagonal phase with (103) orientation is formed. This result suggests that the crystal structure of the nucleating layer

is very important in determining the bulk structure of the deposition film. It would be interesting to see the effect of a cubic nucleating layer deposited by physical vapor deposition.

4.1.3 Crystallite Size of ZnS:Mn Phosphor

XRD data can be used to estimate the grain size of polycrystalline thin films. The Scherrer equation is the simplest formula to calculate crystallite size:

$$B = \frac{C\lambda}{t\cos\theta}$$

where B is the full width at half maximum (FWHM) of the peak, t is the crystallite size, λ is the wavelength of the radiation, θ is one half angle two-theta, and C is a machine modification of about 0.9 -1 value [Cullity, 1978].

Different techniques have also been applied in calculating the crystallite size and microstrain, such as the Warren-Averbach Method [1950] and the Williamson Hall Method [1953]. However, in the former method, the accuracy of calculating microstrain from the XRD result measured by a conventional diffractometer is questionable, due to the limitation of machine and experimental deviation when placing the thin film sample. The Williamson Hall Method can only be applied when at least four peaks are observed. If only a single peak is used in the Williamson Hall method, it reduce to the Scherrer formula (C =1).

In this study, two different ZnS:Mn thin films have been grown. One is the strong preferred orientation with a peak at $2\theta = 28.6^{\circ}$; the others are preferred orientated at $2\theta = 56.4^{\circ}$, with two satellite peaks at $2\theta = 28.6^{\circ}$ and 47.3°. The intensities of these two peaks depend on the processing conditions. To roughly estimate the crystallite size, the Scherrer formula is used in the former case, because only one peak is observed. The lowest value of FWHM was 0.106, which is measured by the line profile method available in the spectrometer software. The profile shape function called pseudo-voigt-1 is chosen to refine the peak shape to obtain the FWHM value. Assuming C = 0.9, the crystallite size is equal to 76 nm when the film thickness is about 6000 Å. This value reasonably compares to the XTEM micrographs (Figure 4-7). This value is smaller than that reported for ALE, but larger than that obtained with others methods [EBE, MOCVD or HTCVD (Mikami, 1991)].

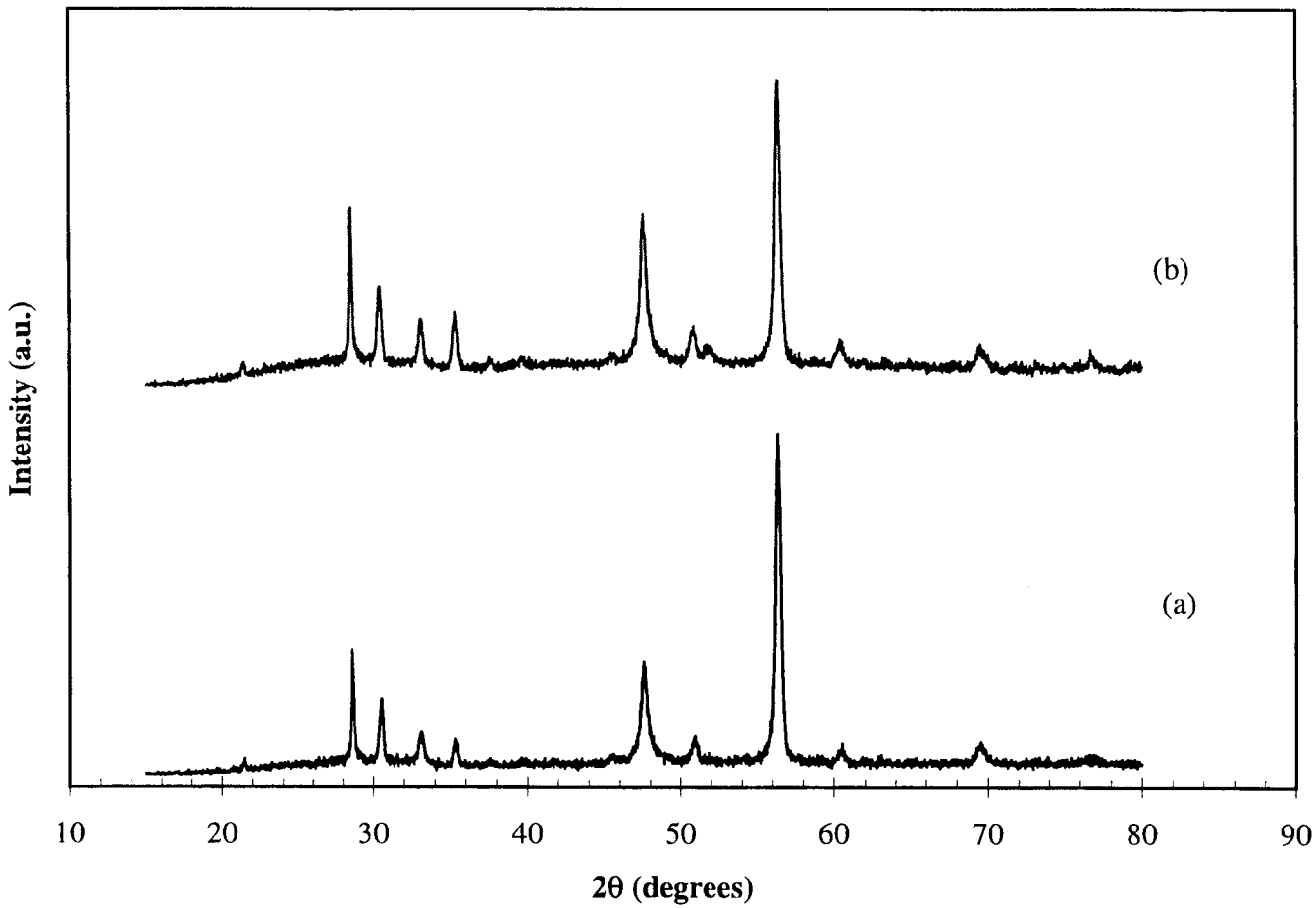

Figure 4-9. The effect of substrate on XRD patterns of ZnS:Mn (a) ATO/ITO/Glass substrate, (b) 200Å ZnS/ATO/ITO/Glass substrate.

4.2 Chemical Characterization of ZnS:Mn Phosphor

As mentioned in Section 2.5, the EL brightness depends strongly on the manganese dopant concentration in the ZnS host material. The Mn concentration is affected by different parameters, such as substrate temperature, source temperature, carrier gas and flow rate. Mn has a negligibly small vapor pressure at 750 °C ($7x10^{-5}$ torr) and is delivered to the reaction chamber through the following reaction:

$$Mn\ (s) + 2HCl\ (g) \rightarrow MnCl_2\ (g) + H_2\ (g).$$

The effect of hydrogen chloride flow rate on Mn concentration is investigated with other reactor parameters fixed. ZnS and Mn source temperatures of 900 °C and 750 °C respectively, and an Ar flow rate of 40 sccm are used. The substrate temperature is 550 °C. The Mn concentration in the ZnS thin films is determined by electron microprobe. The dependence of Mn concentration on hydrogen chloride flow rate is shown in Figure 4-10. It can be seen that the manganese concentration increases with increasing flow rate and abruptly increases at higher flow rate. There are several factors which may contribute to this abrupt increase. The ZnS film thickness depends on HCl flow rate. The XRD spectra of films grown with HCl flow rates of 0.5 - 3 sccm are shown in Figure 4-11. As discussed earlier, film thickness is proportional to the integrated intensity of the XRD spectra. It is obvious that the peak integrated intensity increases a little bit when HCl flow rate increases from 0.5 to 1 sccm. A similar phenomenon was also seen in Mikami's results [1991]; but the mechanism is still not clear. When the HCl flow rate increases up to 2 sccm or higher, the peak intensity decreases very sharply, indicating the growth rate

is significantly reduced. The abundance of HCl leads to "etching" of Zn in less stable surface sites, thus reducing the growth rate. Thinner films result in higher Mn atomic densities. Serving in the complicated role of reactant, carrier gas and etchant, the increasing HCl flow rate causes the non-linear relationship Mn concentration profile.

Most Mn^{+2} ions occupy the Zn^{+2} ion site in the ZnS lattice. Figure 4-12 plots S/Zn ratio and S/(Zn+Mn) ratio vs Mn concentration. The value of S/(Zn+Mn) remains about the same for different concentrations of Mn. However, the value of S/Zn increases as Mn concentration increase, indicating that Zn^{+2} sites are occupied by Mn^{+2} ions.

The surface and bulk chemical composition of ZnS:Mn phosphors were further investigated by AES. Figure 4-13 shows the qualitative determination of which elements are presented in the ZnS:Mn thin layer. The AES spectrum of the near-surface region within 1 - 2 nm from the surface is presented in Figure 4-13(a). Besides the sulfur and zinc elements which appear at 152 and 994 eV, carbon and oxygen are also observed on the surface (272 and 503 eV). These carbon and oxygen impurities are commonly seen on the surface of thin film due to the adsorption of water vapor and CO_2 from the environment. If the material is removed by sputtering the surface with ions, the composition within the thin film can be accessed. AES results after 30 seconds, 2 minutes, and 5 minutes sputtering are shown in Figure 4-13 (b), (c), and (d). The sputtering rate is kept at about 10 Å per second. These three spectra clearly show no oxygen and carbon contamination within the film. The shape and peak intensities of the spectra are almost the same, indicating the same composition across the film. In the spectra, the Mn AES peak was not seen since the Mn concentration was below 0.5% in

this sample and the sensitivity for Mn is just 0.19 comparing to the sensitivity for sulfur, close to the AES detection limit. After 8 minutes of sputtering, the sputtering depth reached into the ATO insulating layer; therefore, Al, Ti, and O elements are observed (27, 51, and 502 eV). Figure 4-14 shows the spectrum of ZnS:Mn phosphor after 2 minutes sputtering, explaining the detailed AES spectrum. The satellite peaks at around 60 and 900 eV comes from Zn element of the LMM auger electron transition type. From the AES study, the ZnS:Mn thin films grown by HTCVD showed no detectable oxygen or carbon contamination.

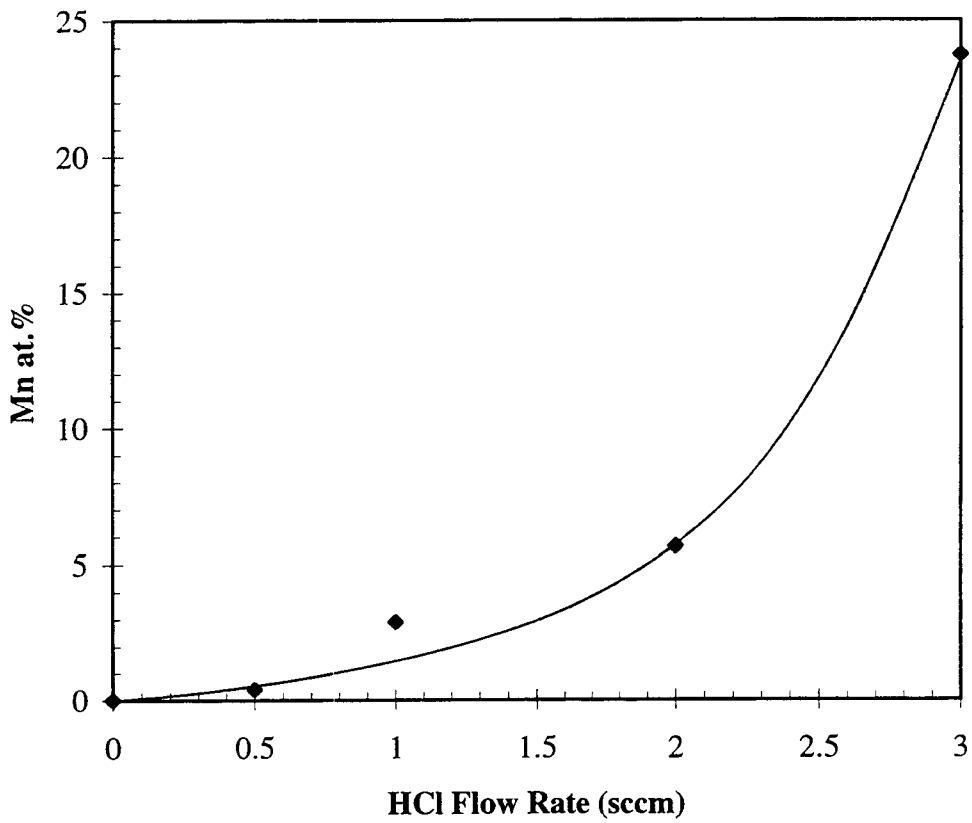

Figure 4-10. The effect of hydrogen chloride flow rate on Mn concentration.

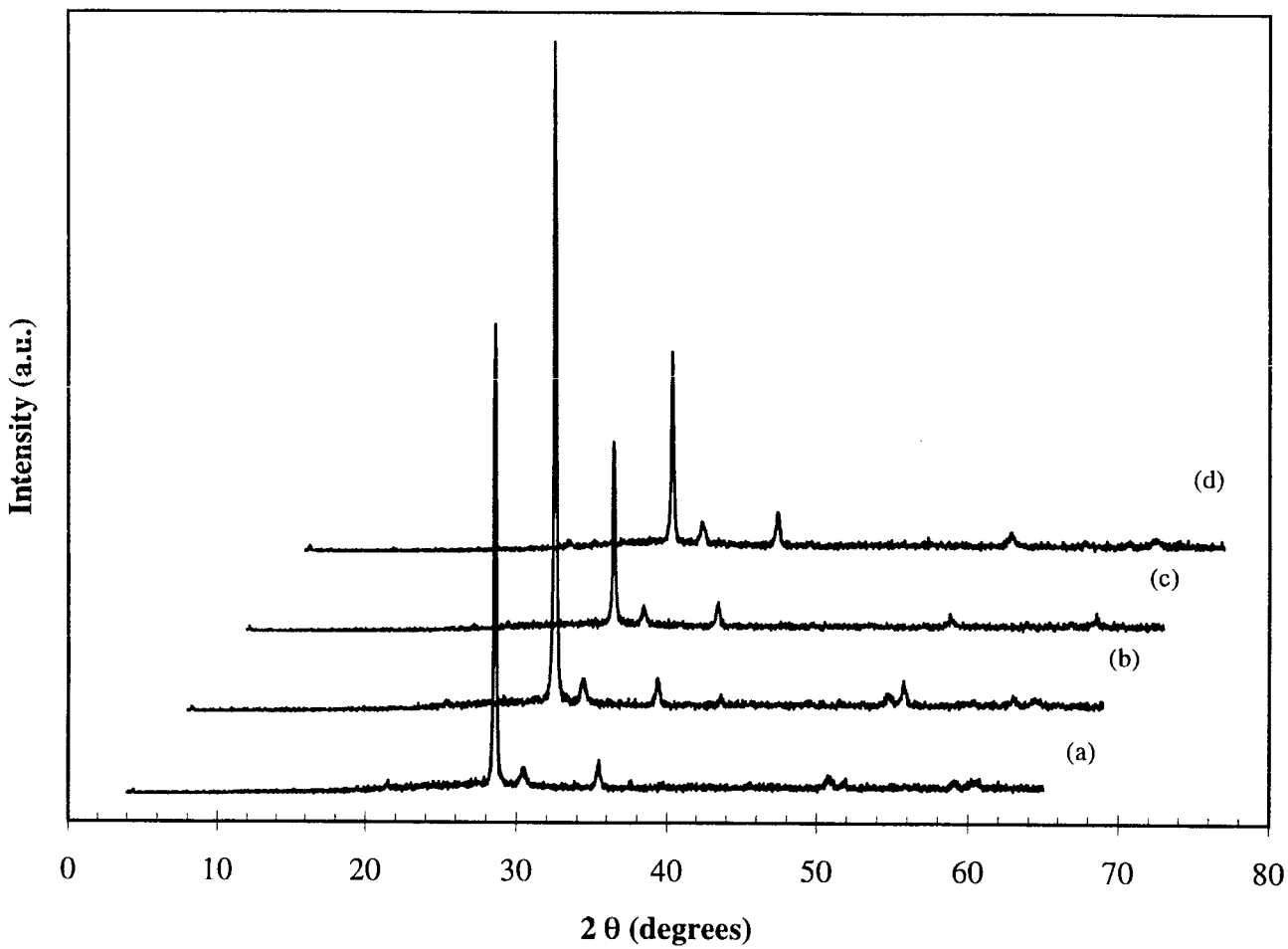

Figure 4-11. XRD spectra of ZnS:Mn films grown with HCl flow rates of: (a) 0.5 sccm, (b) 1 sccm, (c) 2 sccm, (d) 3 sccm.

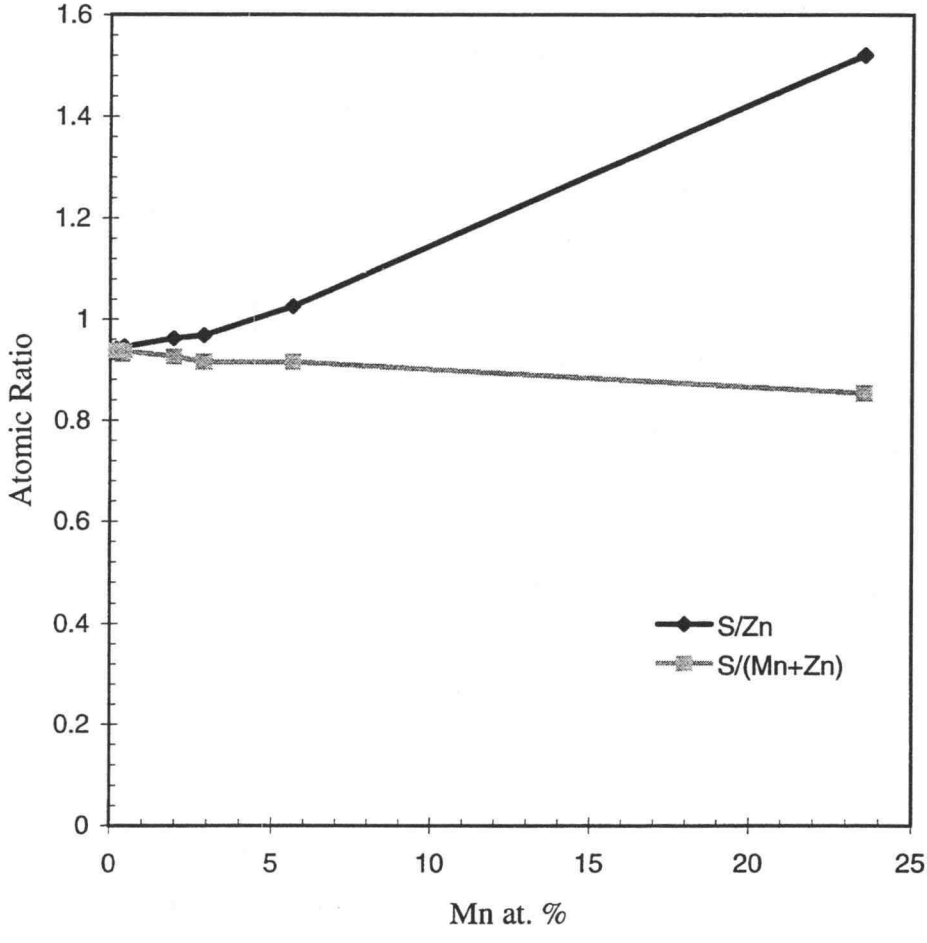

Figure 4-12. The atomic ratio of S to Zn and S to (Zn+Mn) with different Mn concentrations.

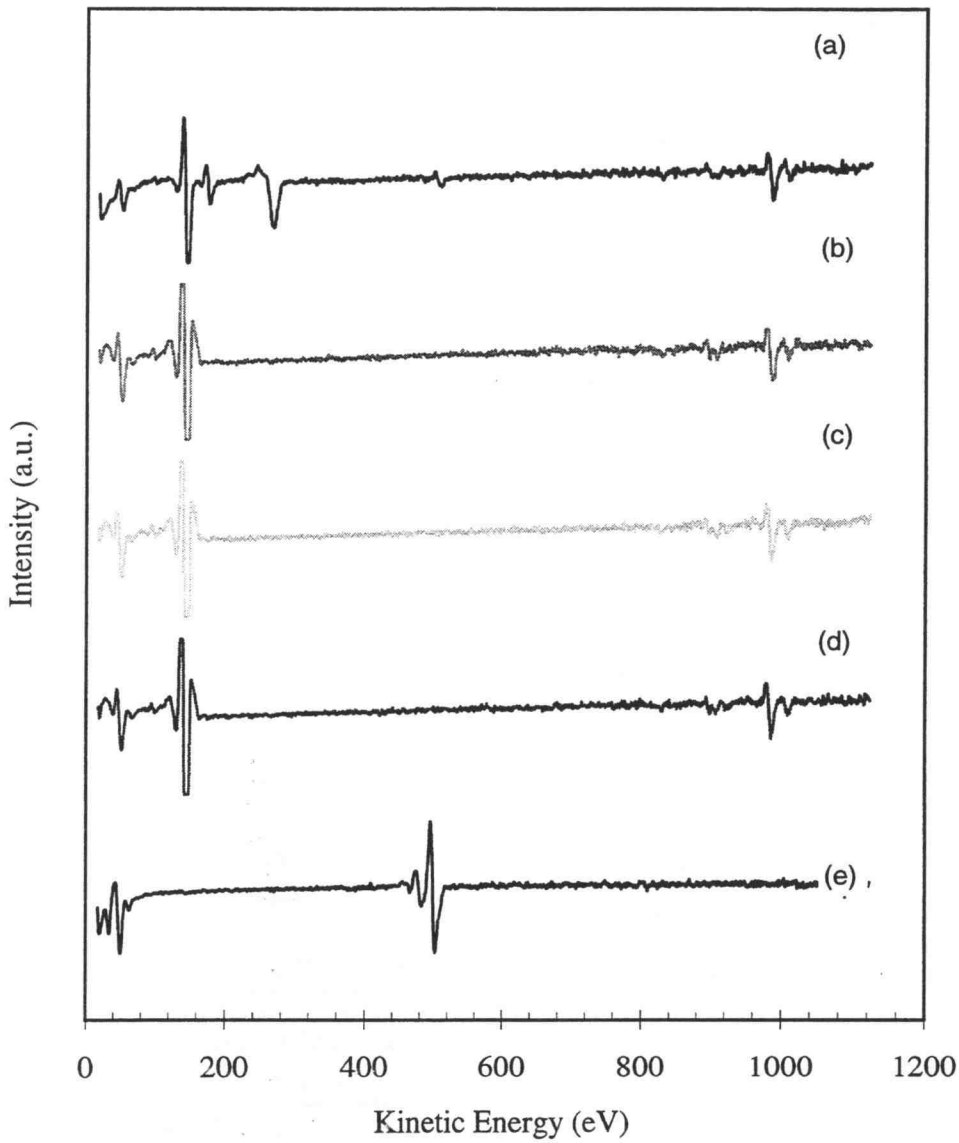

Figure 4-13. Auger Electron Spectroscopy of depth profiling ZnS:Mn :
(a) Fresh surface, (b) 30 seconds sputtering (300Å), (c) 2 minutes sputtering (1200Å), (d) 5 minutes sputtering (3000Å), (e) 8 minutes sputtering (4800Å).

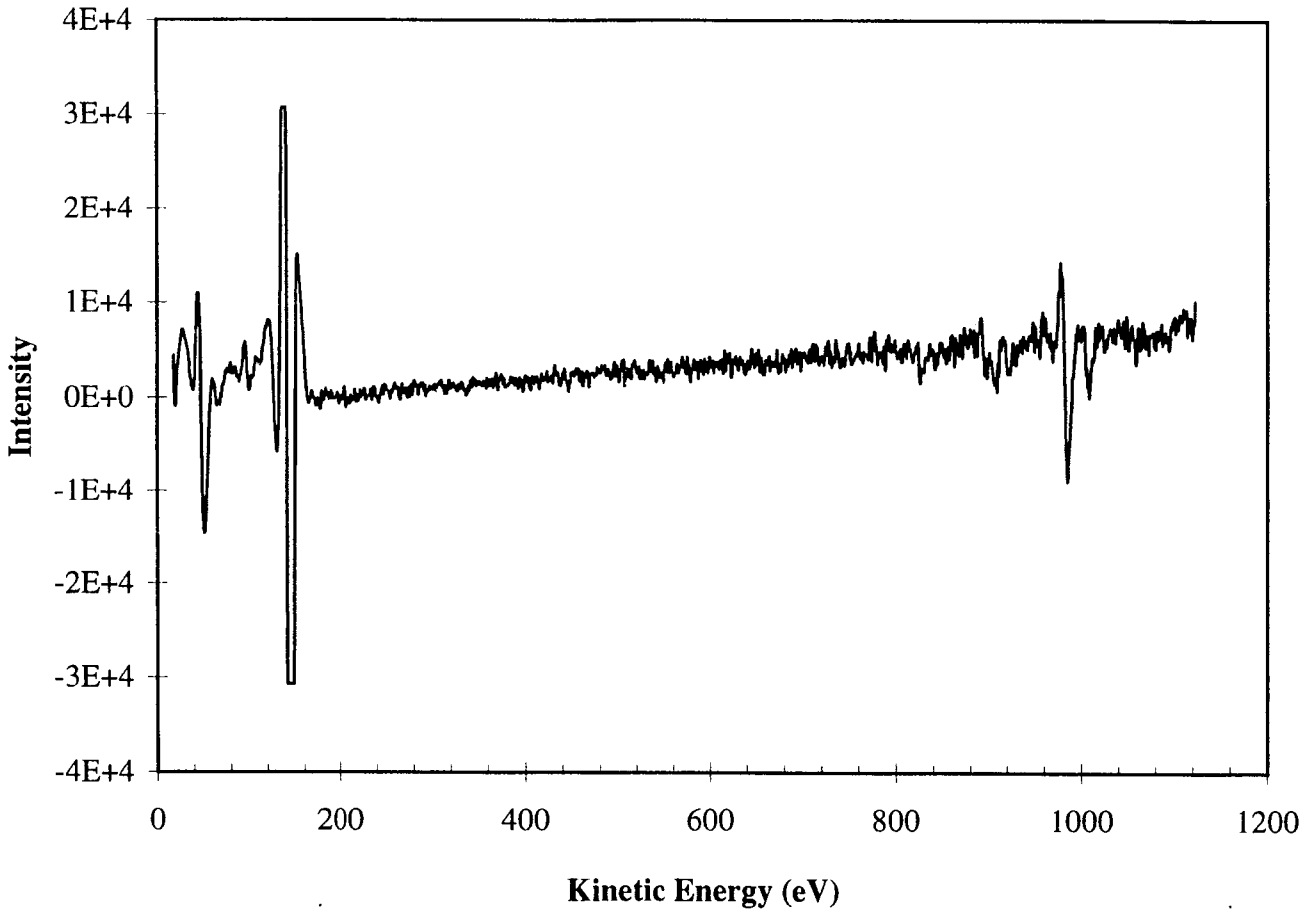

Figure 4-14. AES pattern of ZnS:Mn film after 2 minutes of sputtering. This represents a depth of 1200Å.

Chapter 5

Luminescent Properties of ZnS:Mn and ZnS:Cl film

5.1 Introduction

Wide band gap ZnS thin films are good candidates for host materials in developing EL flat panel displays. Manganese-doped zinc sulfide (ZnS:Mn) which emits at 585 nm is the most successful material for monochrome alternating-current thin film electroluminescent (ACTFEL) devices due to its brightness and high luminescent efficiency. One challenge to increase the EL display market is the production of full-color flat panel displays. Phosphor materials, such as ZnS:Tb,F and ZnS:Sm,F, have shown high green and red luminescence, respectively. Another way of achieving the multicolor is to produce the red and green colors with a filter in front of the broad yellow-orange emission of ZnS:Mn. However, phosphor materials for high blue luminescent efficiency are still lacking. Recently, satellite blue emission in ZnS:Mn thin films has been reported and discussed [Mikami, 1991]. One possibility is that this blue emission may come from chlorine impurities during ZnS:Mn deposition, causing self-activated emission. If the intensity of the blue emission is high enough, the three primary colors for full-color displays may be obtained with a ZnS:Mn/ZnS:Cl phosphor. In this chapter, PL and EL emissions from ZnS:Mn ACTFEL devices are presented. PL with films grown at different substrate temperatures is discussed. Satellite blue PL emissions are observed in

these films as well. A pure blue PL spectra of ZnS intentionally doped with chlorine, measured at different temperatures, is also presented.

5.2 Results and Discussion

5.2.1 Crystalline and Electroluminescent Properties

The experimental conditions for these studies are shown in Table 5-1. A typical XRD is shown in Figure 5-1, showing a polycrystalline film with strong preferred orientation at $2\theta = 28.6^{\circ}$. The hexagonal crystal phase of these films is revealed by the weak diffraction peaks at $2\theta = 30.5^{\circ}$, 39.6°, 51.8°, which correspond to the (101), (102), and (103) hexagonal phase, respectively. By building a ZnS:Mn device (Figure 2-1), EL emission can be measured. Figure 5-2 shows the typical EL emission spectrum of a ZnS:Mn EL device grown by HTCVD. A maximum brightness of 1475 cd/m^2 has been obtained. A more detailed study of the EL emission from these films is presented elsewhere [Husurianto, 1997]. There is no luminescence below the threshold voltage (V_{th}), because the charge is still stored on the interface between the insulator and phosphor layers. The threshold voltage is defined by the voltage corresponding to a luminance of 1 cd/m^2 and is 112 V for this sample. Above the threshold voltage, the brightness increases dramatically with the increase of voltage due to more available hot electrons accelerating and impacting the luminescent centers. The brightness is finally saturated at higher voltages because of the limited activators in the ZnS host material.

The threshold voltage, saturation brightness, and line shape very with processing conditions, driving waveforms, and operation frequencies.

Table 5-1. Reactor Conditions for HTCVD Growth of ZnS:Mn and ZnS:Cl Films.

	ZnS:Mn	ZnS:Cl
Substrate temperature	470 - 580 °C	550 °C
ZnS Source temperature	900 °C	900 °C
Mn source temperature	600 °C	
Total pressure	< 0.2 Torr	< 0.2 Torr
Gas flow rates: Ar	40 sccm	40 sccm
HCl	3 sccm	1.0 sccm

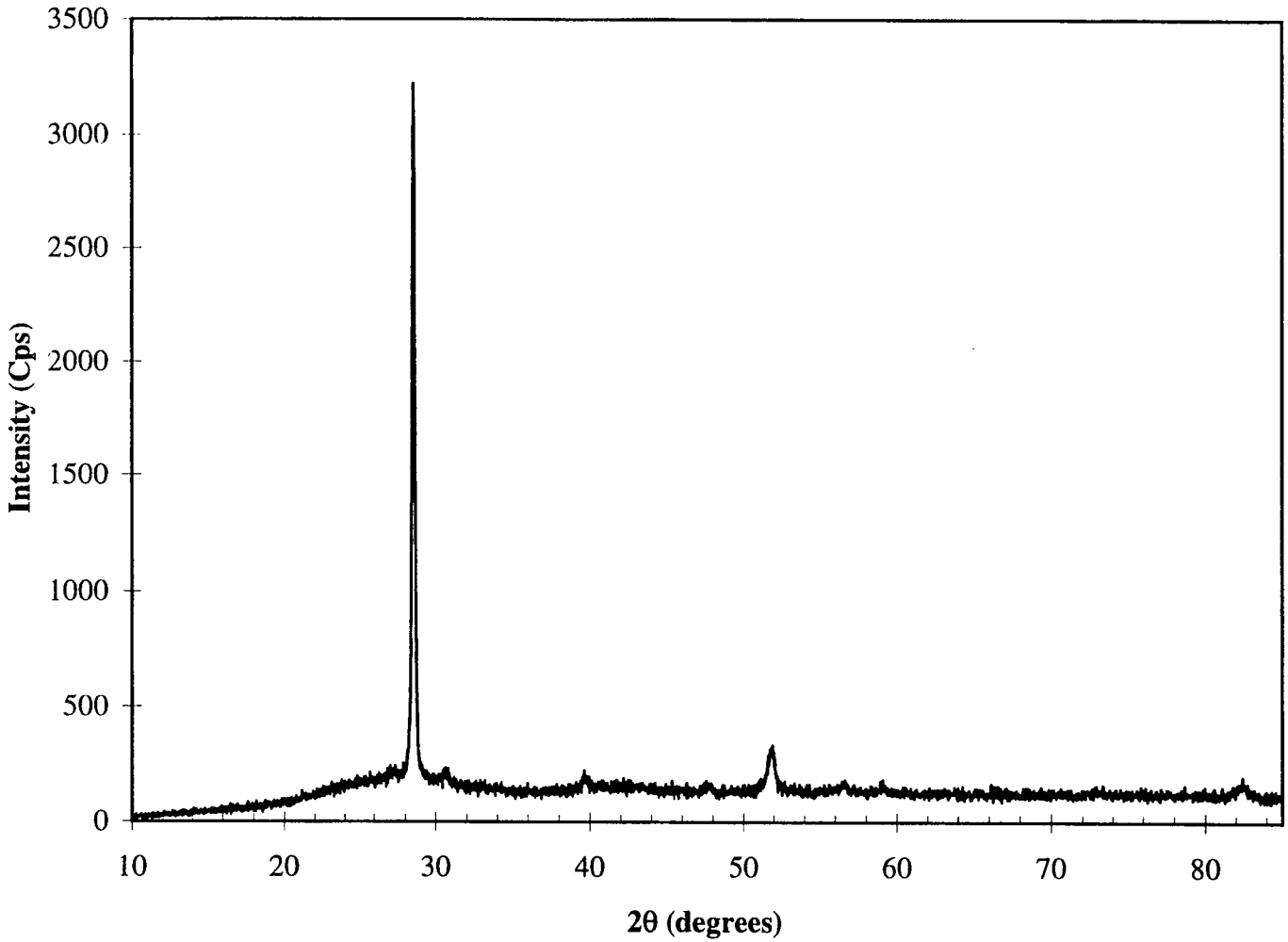

Figure 5-1. XRD of ZnS:Mn thin film.

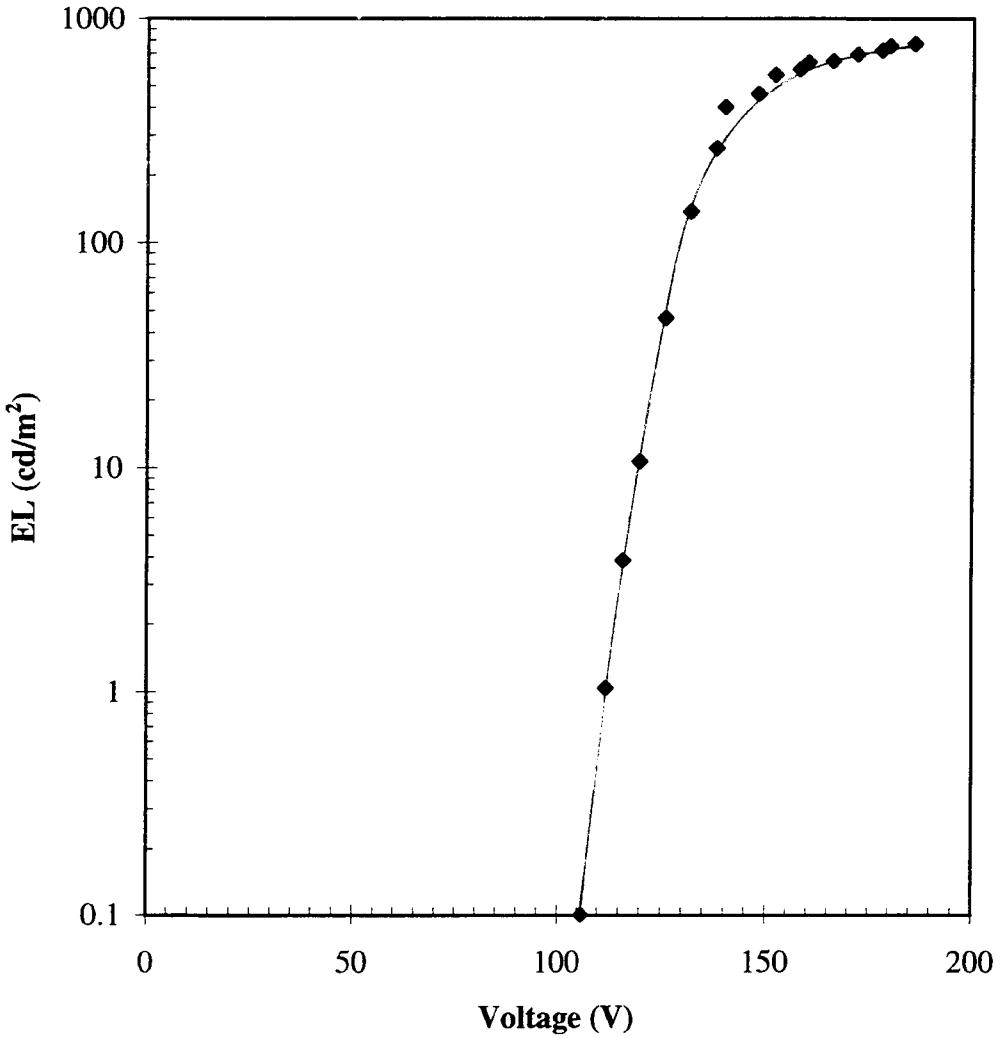

Figure 5-2. ZnS:Mn EL performance vs. voltage.

5.2.2 Substrate Temperature Effect on Photoluminescent Properties

Photoluminescent measurements are made on films deposited directly on bare glass. Therefore, the interference from the ATO and/or the ITO layer is eliminated. Figure 5-3 shows the room-temperature PL spectra of Mn-doped ZnS phosphors at different substrate temperatures. All these films feature emission ranging from yellow-orange to rich orange in color. Figure 5-3(a) presents the spectrum of films grown at 470 °C. The spectrum shows the rich orange color with a peak at 635 nm, which is a higher wavelength from the other three PL spectra. This strong shift to the longer wavelength, from 585 nm to 635 nm, indicates a different luminescent mechanism than those films grown at higher temperature. The PL spectra of films grown at 500 °C, 550 °C and 580 °C are shown in Figure 5-3(b), (c) and (d), respectively. These three films show the dominant yellow-orange emission around 585 nm, which corresponds to the $^4T_1(G) \rightarrow {}^6A_1(S)$ radiative relaxation transition at the Mn center. The PL intensity of the film grown at 500 °C (Figure 5-3(b)) is the highest and about three times higher than the films grown at 550 °C and 580 °C. In addition to the primary yellow-orange emission, the film grown at 500 °C [Figure 5-3(b)] shows satellite blue emission at 445 nm.

Red photoluminescence of ZnS:Mn has been reported in highly doped ZnS crystals in which yellow-orange luminescence decreases are accompanied with the appearance of red emission. Two red emission mechanisms have been proposed. The first explanation was based on the radiationless energy transfer in Mn clusters. When the distance between Mn^{+2} ions becomes close enough, an exchange mechanism leads to the

excited Mn^{+2} ion transferring its energy resonantly to other Mn^{+2} ions and finally to the centers associated with the red emission [Benoit, 1984]. A second explanation is that when the Mn concentration in a ZnS crystal exceeds a critical limit, the MnS phase tends to form [Thong, 1984]. In the MnS phase, Mn, the emitting center, sits in a octahedral site instead of a tetrahedral site. In this case, the energy level of the d orbital of a Mn center is affected by the stronger crystal field in the octahedral coordination than in the tetrahedral coordination. As a result, the energy difference between the $^4T_1(^4G)$ state and the $^6A_1(^6S)$ state decreases. Therefore, the PL emission from Mn activators shifts from yellow to red.

Figure 5-4 shows the electron spin resonance (ESR) spectra of films grown at substrate temperatures of 470 °C, 500 °C and 550 °C. The spectra of the film grown at 580 °C is similar to that grown at 550 °C. In the ESR spectrum of the film deposited at 470 °C, the existence of six well-resolved hyperfine line indicates that the Mn^{+2} centers are isolated in the ZnS host material. The existence of MnS phase of films grown at 470 °C is not detected in either the ESR spectrum or XRD spectra. This result suggests the mechanism for red emission is different than previously proposed. The film grown at a substrate temperature of 500 °C [Figure 5-1(b)] shows six resolved lines with a decrease in peak intensity and an increase in width of each single line. This spectrum is interpreted as arising mostly from isolated Mn^{+2}, but with a higher dopant concentration than in the 470 °C film. A more detailed analysis is presented elsewhere [Lu, 1998]. At 550 °C [Figure 5-4(c)], the six hyperfine lines merge into one unresolved broad line which is assigned to the formation of Mn^{2+} clusters. The line broadening arises from a strong

exchange interaction between Mn^{+2} ions, and indicates a high manganese concentration. As mentioned above, the concentration quenching of the photoluminescence occurs at a higher Mn^{+2} concentration, which causes the decrease of PL intensity seen in Figure 5-3(c). Increased Mn concentrations with increasing substrate temperatures can be explained as follows. At a fixed Mn source temperature, $MnCl_2$ products are formed by the reaction of HCl gas and the Mn source material. After that, the $MnCl_2$ species are transported to the reaction chamber and doped into the phosphor during ZnS thin film deposition. At higher substrate temperatures, $MnCl_2$ is more reactive with ZnS and causes higher doping in ZnS thin films. The overall growth rate increases from 470 °C to 550 °C as well.

In order to confirm that the red photoluminescence of ZnS:Mn thin films grown at 470 °C is not due to Mn clusters or a MnS phase, decay time measurements and electroluminescent characterization have been done on ZnS:Mn ACTFEL devices with the phosphor grown under the same conditions. The result is shown in Figure 5-5. The decay time can be calculated by the following exponential equation [Geoffroy, 1990; Benoit, 1984, 1990]:

$$L / L_o = \exp [-(t / \tau_o)^{\alpha}],$$

where L is luminance intensity, L/L_o is the normalized intensity, τ_o is the decay time, and α is an adjusted parameter. The decay time (τ_o) and α vary with Mn concentration. In general, the Mn concentration is lower than 0.4 mole% when the decay time is larger than 1000 μs. The value of α range from 1 to 0. α is equal to 0.5 or lower when there is dipole-dipole interaction. The value of decay time and α, shown in Figure 5-5, are 1350

μs and 0.76. The decay time value shows that the Mn concentration is low and there are no Mn clusters in the sample. It is interesting that the EL measurement shows yellow-orange emission instead of red emission for the sample grown at 470 °C. The peak EL emission occurs at 582 nm.

The PL red emission pattern has been deconvoluted into two lines with domain peaks at 633 nm and 595 nm. The resulting lines are show in Figure 5-6. Zhang et al. [1989] proposed an excitation mechanism model for explaining the relative intensity of EL and PL emission, but did not explain a change in color. Borisenko [1992] reported that red emission with a peak at 600 nm is possible if the Mn ion sits at an octahedral interstice in the ZnS lattice. However, since this film is grown at low substrate temperature, an interband defect may play a role in the red photoluminescence. The mechanism is still under study.

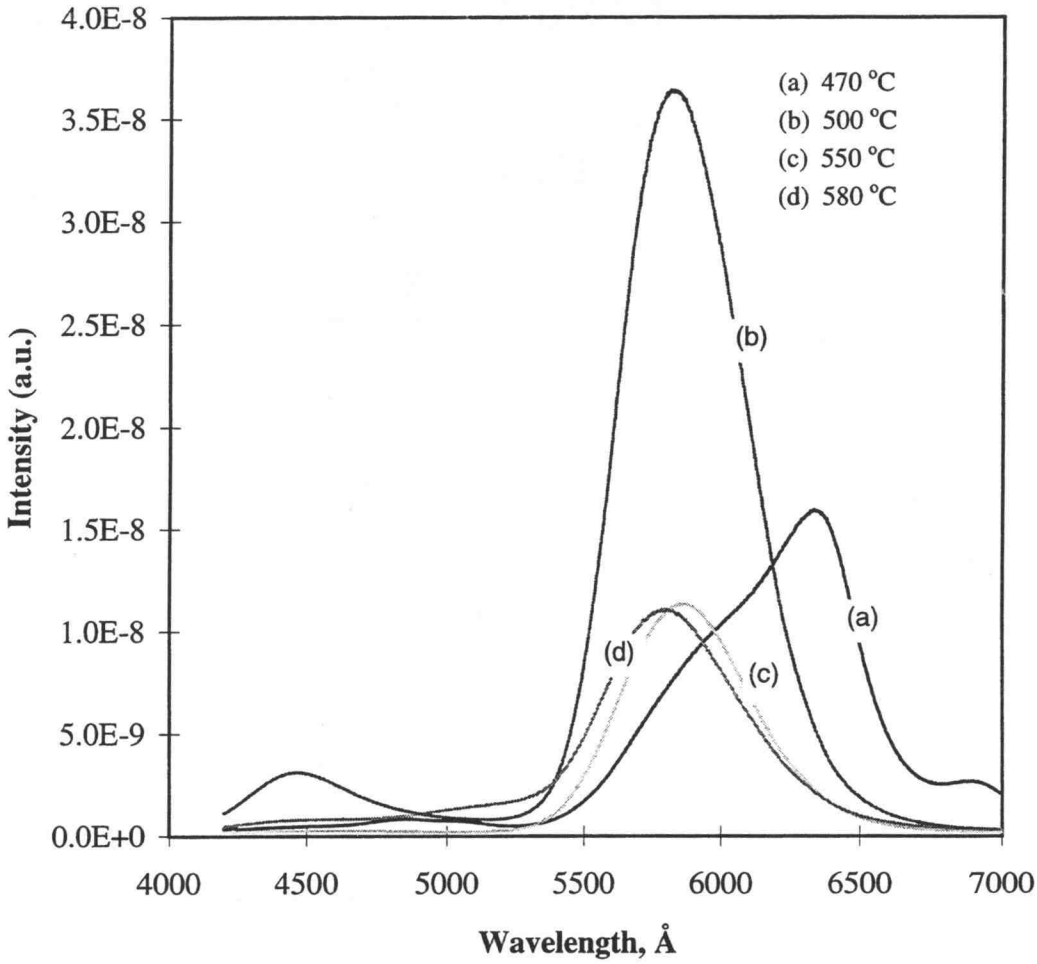

Figure 5-3. Photoluminescence vs. substrate temperature of films grown with substrate temperatures of (a) 470 °C, (b) 500 °C, (c) 550 °C, (d) 580°C with a fixed excitation wavelength 330nm.

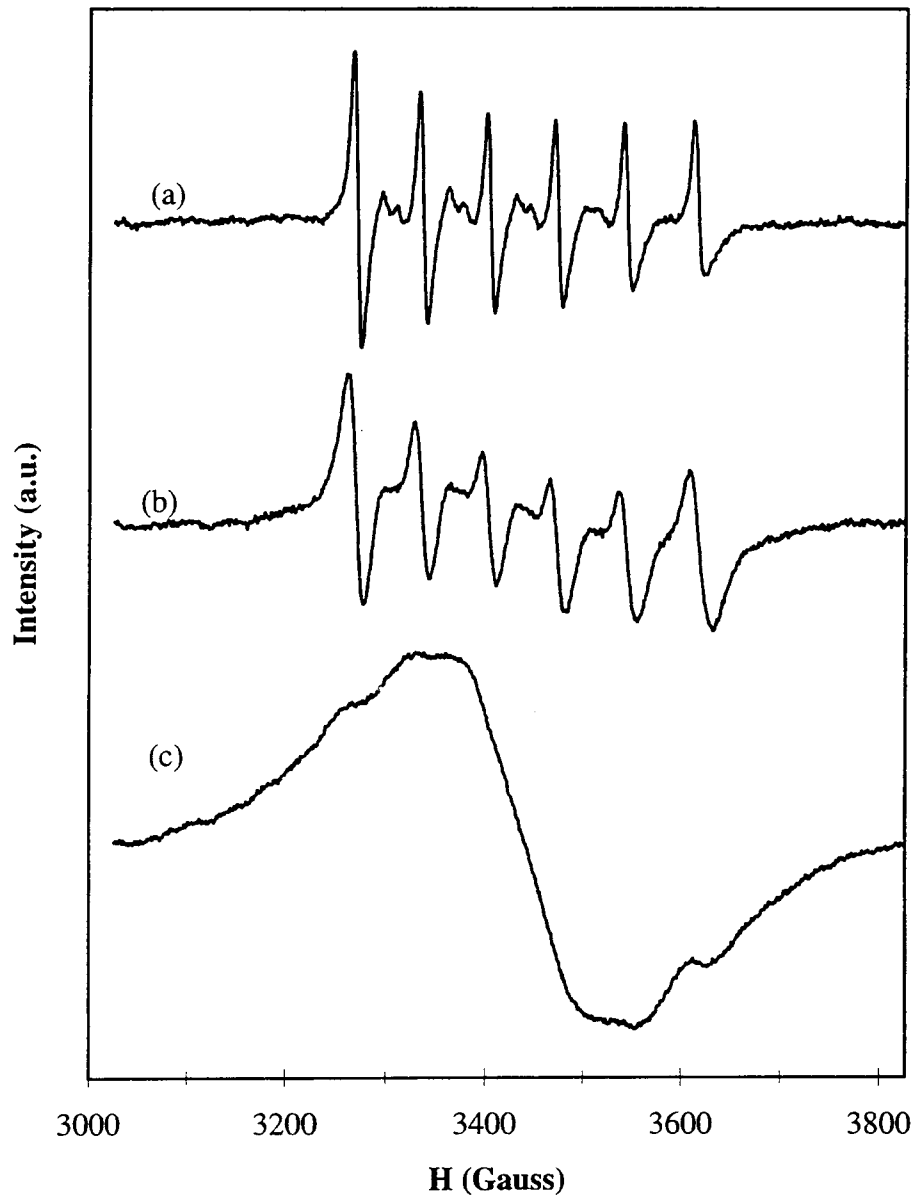

Figure 5-4. ESR spectra of ZnS:Mn films grown at different substrate temperatures of (a) 470 °C, (b) 500 °C, (c) 550 °C.

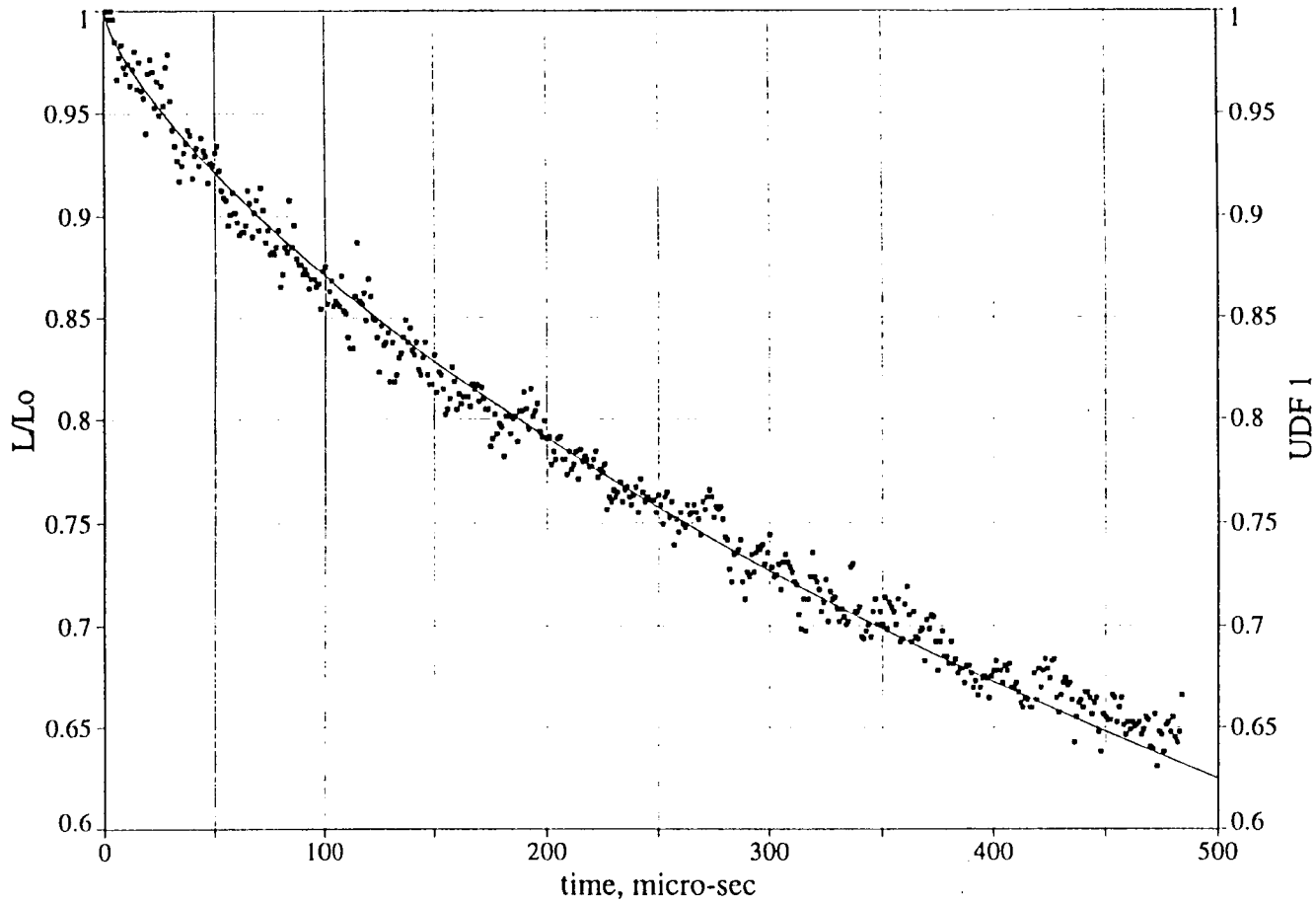

Figure 5-5. Electroluminescent decay measurement and fit of a ZnS:Mn film grown at a substrate temperature of 470 °C.

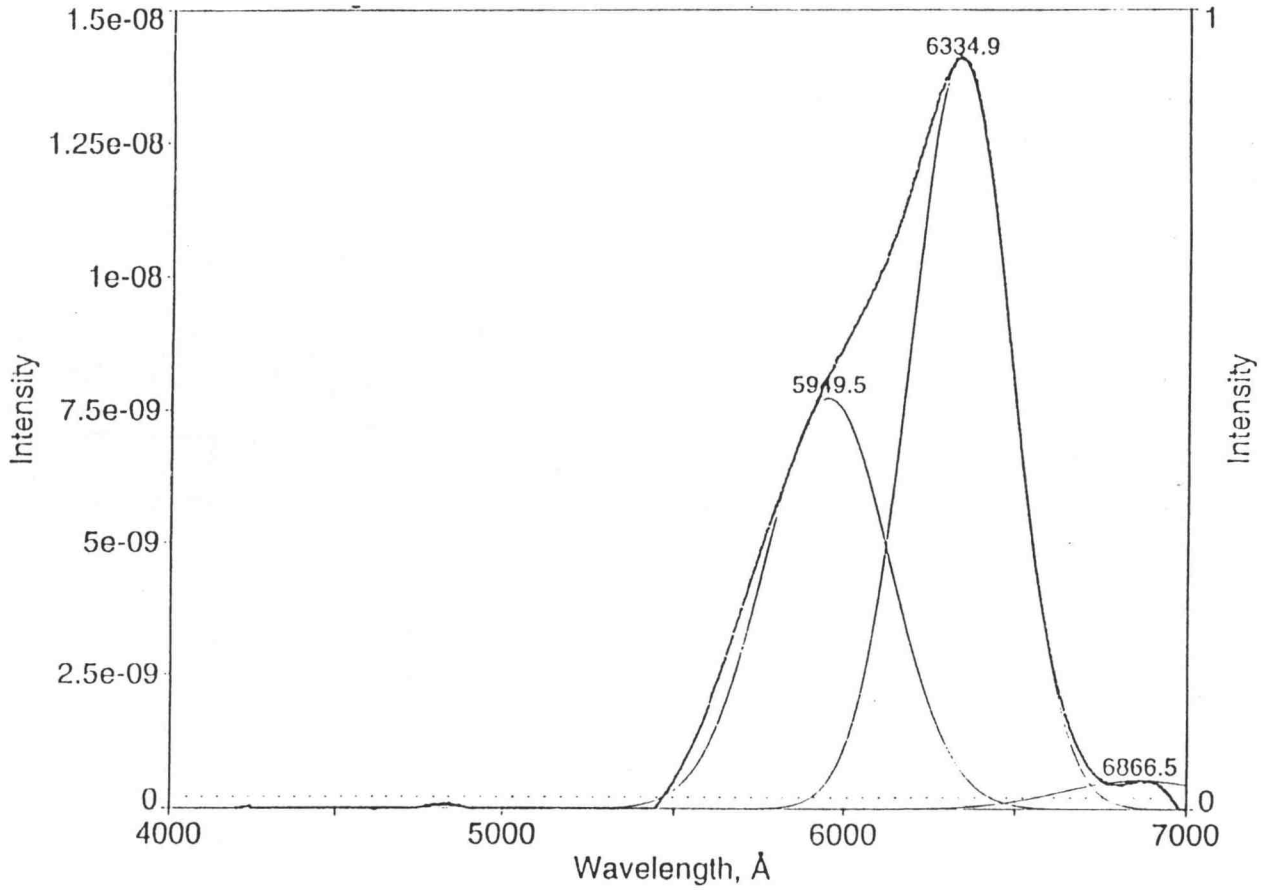

Figure 5-6. Deconvolution of red PL spectra into 2 spectra with peaks at 595 nm and 633.4 nm.

5.2.3 Photoluminescent Properties of ZnS:Cl Phosphor

ZnS:Cl is prepared in an attempt to achieve self-activated blue emission which has been seen in ZnS:Mn films [Figure 5-3(b)]. Growth conditions are shown in Table 5-1. Emission and excitation spectra of PL measurements are at room-temperature and 12 K are shown in Figure 5-7. At room temperature, this film exhibits a strong blue emission, peaking at 462 nm. This brightness is comparable to the yellow-orange emission shown in Figure 5-3. The excitation spectrum increases steadily to a peak at 328 nm and then drops precipitously at a value around that of the ZnS band gap, suggesting a band-to-band excitation mechanism. Thus, significantly hotter electrons are needed to excite the blue ZnS:Cl than the yellow orange ZnS:Mn. On cooling the film to 12 K, the PL intensity increases by a factor of 3 due to the higher excitation absorption efficiency. Also, the main blue peak shifts to lower energy, 470 nm. Thomas et al. [1984] reported shifts, both of lower and higher emission energy, of self-activated emission in ZnS due to the different Cu impurity concentrations. The detailed explanation of different occupation sites of Cu, such as substitutional or interstitial sites, at different concentration levels associated with pair emission was proposed [Thomas, 1984; Era, 1968]. Emission shifts at different temperature are also affected by the increase of band gap of the host material or the position change of the energy level of the dopant in band gap when cooling. In Figure 5-7, there is also seen a constant emission in the red end of the spectrum at cool temperatures. This emission may be associated with the release of electrons/holes from a shallow level to the conduction/valence at 12K, which is thermally quenched with

nonradiative absorption and relaxation at room temperature. The excitation pulse, measured by fixing at the blue emission peak, looks similar to that at room temperature, but shows more features. Figure 5-8 presents an energy band diagram for self-activated emission associated with Cl donors on the sulfur site (Cl_S) and Zn vacancy (V_{Zn}) acceptor. The actual positions of these donor and acceptor energy levels are still unclear. The different ionization energy for V_{Zn} and Cl_S have been estimated. The first ionization energy of V_{Zn} ($V_{Zn}^{'}$) in ZnS have been estimated to be 0.5 eV [Wager, 1996] or 0.58 eV [Georgobiani, 1981], positioned above the valence band edge. The latter ionization energy estimation is based on the electrical-conductivity activation energies and the dependence of the photoconductivity. The ionization energy of Cl_S in ZnS was estimated to be as 0.25 eV [Kasai, 1962]. Based on the above and the 3.6 eV ZnS band gap, the 2.77 eV of donor-acceptor emission is obtained. However, this may shift slightly due to other defects, such as sulfur vacancies, interstitial site occupation of chlorine, and impurities. The peak SA emission of ZnS:Cl films in Figure 5-7 corresponds to a difference between energy levels of around 2.7 eV, 460 nm. Those defects may also explain the different blue emission peaks from 445 nm (Figure 5-3(b), Mn impurities within ZnS thin film) to 460 nm (Figure 5-7).

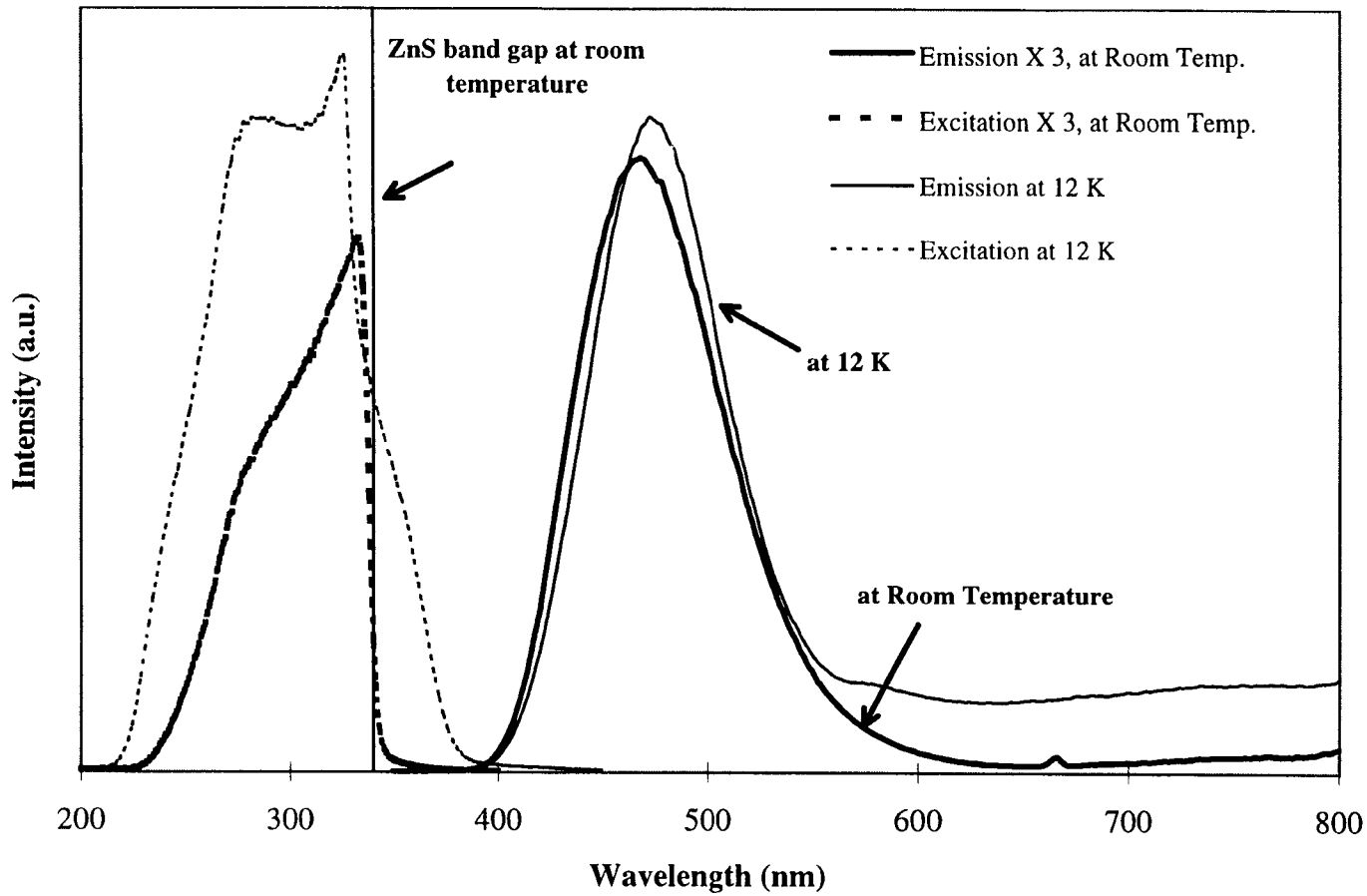

Figure 5-7. Photoluminescence excitation and emission of ZnS:Cl thin film.

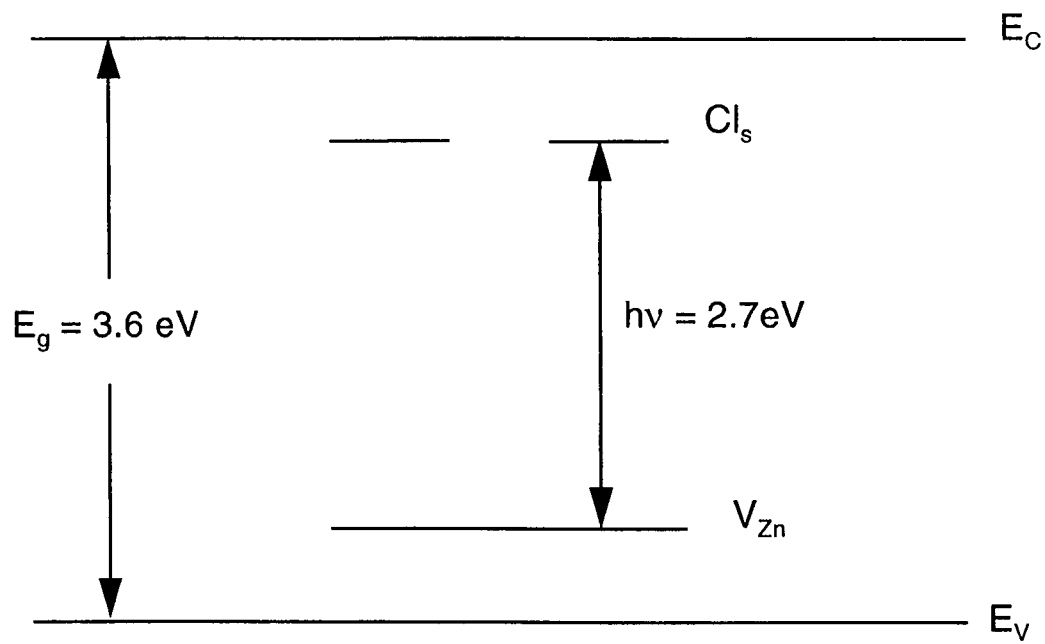

Figure 5-8. Energy states associated with blue (SA) emission of ZnS:Cl thin film.

Chapter 6
The Effect of Processing Conditions on Crystal Orientation and Structure in ZnS:Mn Thin Films

6.1 Introduction

Manganese-doped zinc sulfide (ZnS:Mn) thin-films have played a central role in the development of alternating-current thin-film electroluminescent (ACTFEL) devices. This material has been extensively synthesized by a variety of techniques including: electron beam evaporation [Hurd, 1979; Ono, 1995], sputtering [Xian, 1994], atomic layer epitaxy (ALE) [Suntola, 1992], metalorganic chemical vapor deposition (MOCVD) [Migita], and halide-transport chemical vapor deposition (HTCVD) [Mikami: 1991, 1992]. Among these methods, HTCVD is attractive due to its capability of producing electroluminescent films with large crystal grains, bright luminescence, and excellent aging stability [Mikami: 1991, 1992]. Additionally, HTCVD is potentially well suited to low-cost, large-area deposition.

One challenge for ACTFEL devices is to improve the efficiency of electroluminescence. Poor efficiencies can be caused by poor crystal quality, a deficient number of hot electrons for impact excitation, or a small collision cross section for excitation of the luminescent center [Ono, 1995]. The efficiency of ZnS:Mn electroluminescent (EL) devices can be improved by increasing the crystallite size. However, the influence of crystal structure, such as crystal phase, crystallographic orientation, and the local structure of the luminescent center within the ZnS host, on the

efficiency of EL devices is still under discussion. ZnS:Mn thin-films exhibit strongly preferred orientation in the (111) direction for the cubic phase or the (002) direction for the hexagonal phase, regardless of the deposition process [Mikami, 1991; Tanninen, 1983]. In this paper, we report a different preferred orientation, (311), for the cubic films deposited by HTCVD and examine the effect of the crystal structure and orientation on the electrical properties of the device.

6.2 Results and Discussion

The experimental conditions are shown in Table 6-1. The XRD patterns of Mn-doped ZnS phosphors with different growth conditions are presented in Figure 6-1. The addition of H_2S has a profound effect on crystal structure and orientation. The first two films, shown in Figure 6-1(a) and (b), are grown without H_2S present in the reactor. The substrate temperatures are 500 °C and 550 °C, respectively. Both films show a strong peak at $2\theta = 28.6^\circ$, indicating oriented growth. Both spectra also exhibit peaks at 39.6° and 51.8°. These latter peaks clearly reveal a hexagonal phase since they correspond to the (102) and (103) hexagonal phase directions, respectively. These peaks are absent in the diffraction patterns of cubic films. The other satellite peaks at $2\theta = 21.4^\circ$, 35.5°, 50.8°, and 60.5° belong to the ITO layer. The peak at $2\theta = 30.5^\circ$ may be due to the overlap of the (101) hexagonal phase peak and another from the ITO layer. The spectra presented in Figure 6-1(c), (d), and (e), are from films grown on substrates with only amorphous ATO to eliminate the interference from ITO. These three spectra, Figure 6-

1(c), (d) and (e), are of films that are grown in a H_2S environment. Figure 6-1(c) and (d) are spectra from films grown at a substrate temperature of 550 °C and a H_2S flow rate of 0.4 sccm but with ZnS heater temperatures of 940 °C and 980 °C, respectively. In these films, the peak at 56.4°, corresponding to the (112) direction of the hexagonal phase or (311) direction of the cubic phase, becomes more pronounced indicating a shift in the preferred orientation. Additionally, peaks at 33.1° and 69.4°, corresponding to (200) and (400) directions, emerge while the peak at 51.8° diminishes [Figure 6-1(c)] until it is not detectable [Figure 6-1(d)], indicating a cubic (or mainly cubic) phase. The fifth film is grown at 500 °C and shows the largest fraction under the peak at 56.4°. Again there are cubic peaks at 33.1° and 69.4° and no hexagonal peak at 51.8°. The change in the processing conditions affects both the phase of the resulting film as well as its orientation. In some cases, growth can be altered from that with the most dense atomic plane parallel to the growth surface (28.6°) to the less dense (56.4°) plane associated with cubic (311) oriented growth.

Introduction of a H_2S ambient in the reactor has two effects which may help promote (311) growth. It increases the flux of S containing species to the substrate, and it also introduces a different chemical species, H_2S rather than S_2. Growth along the most dense atomic plane [(111) or (002)] proceeds by alternating layers of one species followed by the other. We propose that most HTCVD processes grow in this manner since the less volatile Zn atoms are likely to form the initial layer. The stability of the ZnS bond drives the dissociation of S_2 and incorporation of sulfur into the film. Growth in the (311) direction is along atomic planes populated by both Zn and S. The increased

sulfur flux and addition of a single bonded sulfur species could allow the sulfur to effectively compete with Zn in the nucleation of the phosphor thin-film, leading to growth along a less dense plane populated by both species.

Electron spin resonance (ESR) spectra of a (311) oriented thin-film grown in a H_2S environment and a (002) oriented film grown at identical reactor conditions, except without H_2S present, are shown in Figure 6-2. Both spectra show six well resolved hyperfine lines due to isolated Mn^{2+} centers which have nuclear spin, I=5/2 [Kreissel, 1986; Kennedy, 1995]. However there is also fine structure present in the (002) oriented film. This structure is absent in the (311) film indicating a different local crystal field. The zero-field splitting parameter, D, in the spin Hamiltonian gives rise to fine structure. This parameter is non-zero only in environments with symmetries lower then cubic. Therefore, for Mn^{2+} centers occupying a cubic site, no fine structure splitting is observed. However, for Mn^{2+} centers in a lattice with hexagonal crystal structure, some weak fine-structure lines appear, as shown in Figure 6-2(b), corresponding to the transitions between M_S=1/2 and M_S = -1/2 at $\Delta M_I = \pm 1$.

The Q-F_P curve of an EL device with a cubic (311) oriented phosphor film, grown in a H_2S environment, is shown in Figure 6-3. The conduction charge (Q_{cond}), the total charge which is transported across the phosphor during a voltage pulse, is illustrated for the case when the device is driven 60 V above threshold. Conduction charge is proportional to the number of electrons which tunnel out of trap states located at the ZnS/insulator interface. Therefore, the conduction charge is sensitive to the distribution of interface energy states. In this case, the value of Q_{cond}, 5.0 $\mu C/cm^2$, is twice as large as

the (002) film grown under identical conditions, but without H_2S. A larger conduction charge translates into more electrons available to excite luminescent centers and, consequently, leads to more efficient EL devices. Both films have a value of approximately 0.11 for the full width at half maximum (FWHM) of their primary XRD peak, indicating they have similar crystal quality and grain size. While space charge may provide some difference in Q_{cond}, it is unlikely to account for a factor of 2.

Table 6-2 compares electrical properties of these two devices and also includes ALE and evaporated ZnS:Mn films reported in the literature. The (311) film has a conduction charge similar to the ALE film and greater than the evaporated film. Note that the ALE film is hexagonal while the evaporated film is cubic, in contrast to the HTCVD films in which the cubic phase shows more conduction charge. Moreover, the leakage charge, Q_{leak}, of the (311) HTCVD films is small compared to the other devices. The small value of leakage charge indicates that the shallow interface states in (311) oriented ZnS:Mn may not be populated, i.e., there are enough deeper energy levels to store the polarization charge during the zero bias portion of the waveform. This is another indication that there are a greater number of interface states associated with the (311) oriented films. The less dense growth plane of the (311) films appears to lead to more available interface states. This could be due to the less dense atomic phosphor layer at the insulator surface and the contribution of surface microfaceting of the higher Miller index surface to the atomic disorder at the phosphor/insulator surface.

Table 6-1. Reactor conditions for HTCVD growth of ZnS:Mn films.

Substrate temperature	500 - 550 °C
ZnS source temperature	900 - 980 °C
Mn source temperature	725 °C
Total pressure	< 0.2 Torr
Gas flow rates: Ar	40 sccm
H_2S	0.4 sccm
HCl	0.5-1.0 sccm

Table 6-2. Electrical properties of ACTFEL devices at 60 V above threshold in which ZnS:Mn films are deposited by HTCVD, ALE and evaporation. These parameters are measured using the Q-F_p technique.

Measured parameter		HTCVD		ALE	Evaporated
		(311)	(002)	(002)	(111)
F_{ss}	(MV/cm)	1.7	1.6	2.1	1.7
Q_{cond}	($\mu C/cm^2$)	5.0	2.3	5.0	2.8
Q_{leak}	($\mu C/cm^2$)	0.1	0.5	1.3	0.3
Q_{relax}	($\mu C/cm^2$)	1.7	0.6	2.1	1.0
Q_{pol}	($\mu C/cm^2$)	2.4	0.9	1.9	1.3

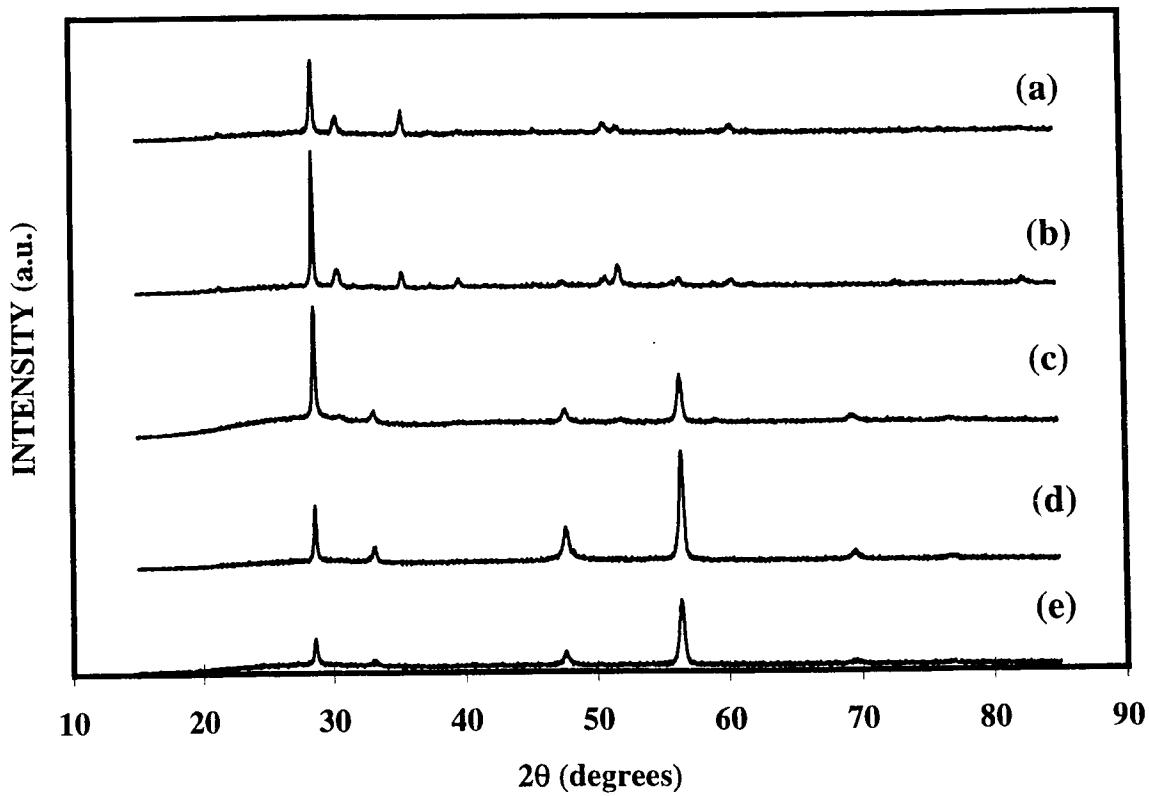

Figure 6-1. X-ray diffraction pattern of ZnS:Mn films grown under the following reactor conditions: (a) substrate temperature 500°C, without H2S, Tzns = 900°C, (b) substrate temperature 550°C, without H_2S, Tzns = 900°C, (c) at 550°C, with H_2S, Tzns = 940°C, (d) at 550°C, with H_2S ambient, Tzns = 980°C, (e) at 500°C, with H_2S ambient, Tzns = 940°C.

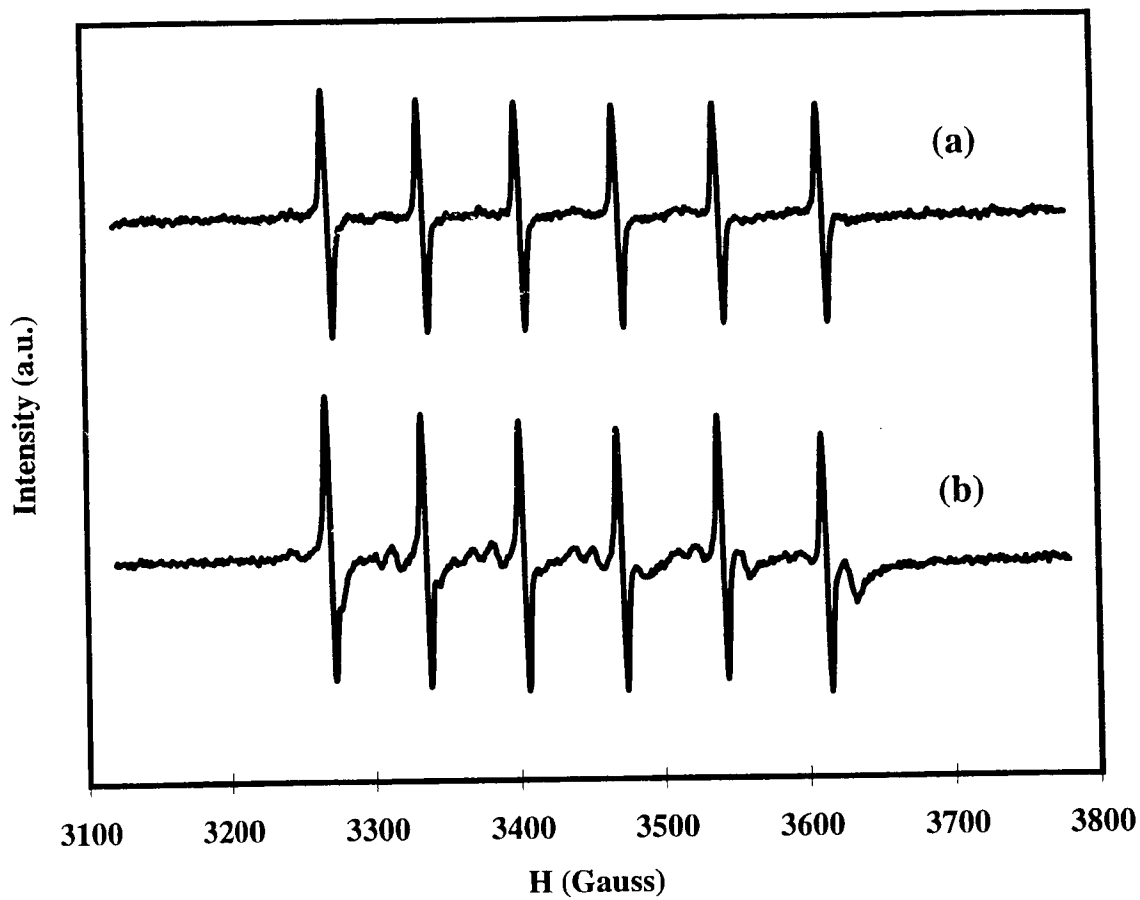

Figure 6-2. ESR spectra of ZnS:Mn films with preferred orientation which corresponds to an XRD peak at (a) $2\theta = 56.4^{\circ}$ and (b) 28.6°. These films are grown under identical reactor conditions except that the film in (a) is grown in a H2S ambient.

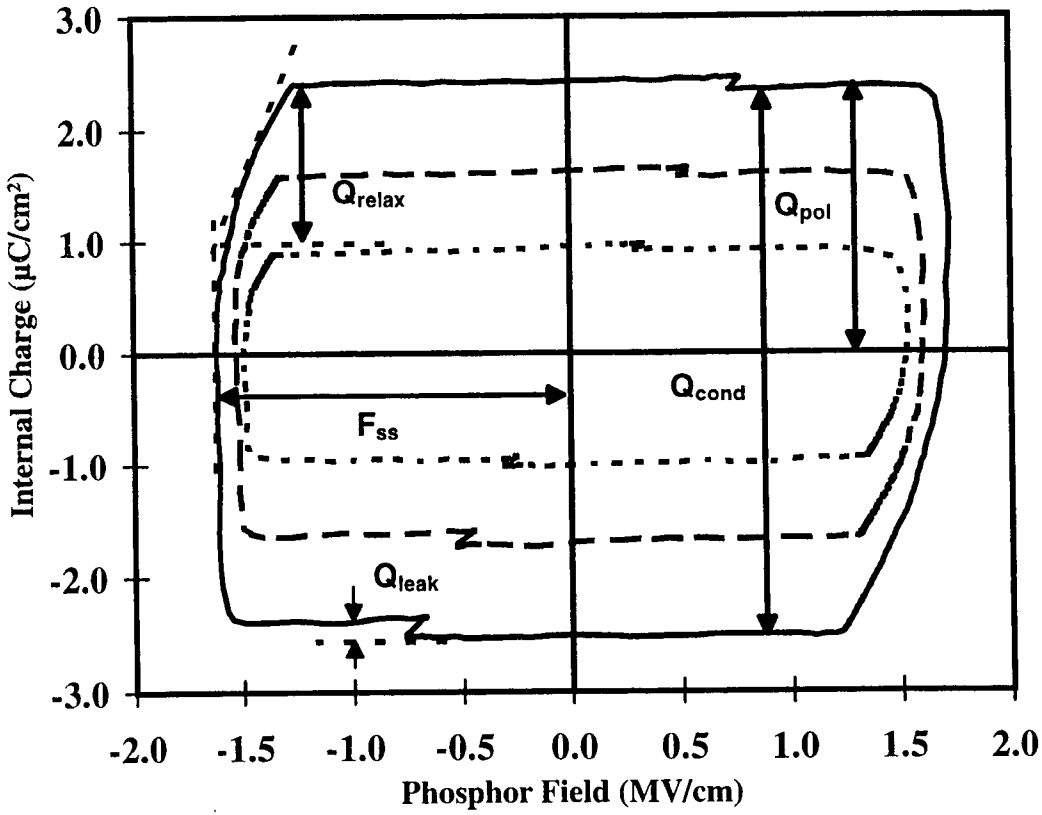

Figure 6-3. Q-Fp curves of ZnS:Mn ACTFEL devices with a (311) preferred oriented growth. Vmax at 20, 40, 60 V above threshold voltage. The conduction charge, Q_{cond}, the leakage charge, Q_{leak} the relaxation charge, Q_{relax}, and the polarization charge, Q_{pol}, which are reported in Table 6-2, are indicated on the figure.

6.3 Summary

By increasing the concentration and varying the chemical nature of the sulfur-containing species in the HTCVD reactor, the orientation of the ZnS:Mn films can be changed to grow in the less dense (311) direction. This results in a phase change from hexagonal to cubic and a change in the local Mn^{2+} crystal environment. Furthermore, the amount of conduction charge which moves across the phosphor during a voltage pulse doubles.

Chapter 7

Conclusions and Recommendations for Future Work

7.1 Conclusions

The work presented in this thesis is performed in an attempt to develop better phosphor processing methods and materials for ACTFEL devices. In pursuit of this goal, a halide transport chemical vapor deposition system is used to grow ZnS:Mn EL phosphors. The results of this work are summarized as follows:

1. Crystal growth of ZnS at 550 °C is controlled by surface reaction.
2. Without H_2S present, cubic undoped ZnS grown by HTCVD is dominant below 600 °C, while ZnS:Mn films exhibit hexagonal crystal structure.
3. Crystal size increase as films grow, which may explain the non-symmetry of positive and negative pulses in ZnS:Mn ACTFEL device.
4. The crystal structure of the nucleating layer is very important in determining the bulk structure of the deposited film.
5. The largest average crystallite size obtained is around 76 nm.
6. The complicated role of reactant, carrier gas, and etchant for HCl in HTCVD system may explain the non-linear relationship of the Mn concentration profile.
7. Most Mn^{+2} ions occupy the Zn^{+2} ion site in ZnS:Mn films.

8. A maximum EL brightness of 1475 cd/m^2 at an excitation frequency of 1 KHz using bipolar voltage pulses is achieved.
9. The difference in PL intensity of ZnS:Mn films grown at different substrate temperature correlates with the Mn concentration. Red emission, seen in films grown at 470 ^{o}C, is not caused by Mn clusters.
10. ZnS:Cl thin films are deposited and show a prominent blue (462 nm) photoluminescence associated with self-activated emission.
11. Growth of ZnS:Mn thin films in H_2S ambient can change the crystal structure from hexagonal to cubic and the preferred orientation of growth from (002) to (311).
12. When grown is in the (311) direction, as compared to the (002) direction, the conduction charge increases by a factor of two.

7.2 Recommendations for Future Work

Future work are recommended in several direction:

1. Investigation the of kinetics and thermodynamics of the adsorption/desorption process to be able to understand and easily control the different oriented growth and the amount of dopant (especially for (311) preferred oriented film). The installation of mass spectroscopy onto the HTCVD system is recommended.
2. The effect of crystal structure on EL performance can be studied by applying nucleating layer.
3. Measure decay time as a function of temperature for the red emission sample.
4. EL study of (311) preferred oriented ZnS:Mn device: optimize the Mn concentration, investigate the aging study, and compare the aging of (002) and (311) film.
5. ESR study:
    I. Calculate Mn concentration quantitatively.
    II. It would be interesting to compare fresh and aged ZnS:Mn phosphors (could be ALE film, HTCVD film, or sputtering film). If the aging is associated with the decrease of brightness or Mn diffusion, it should be detected in the ESR spectra.
    III. Study the effect of annealing on Mn distribution in the ZnS film.

REFERENCE

Abu-Dayah, A., and J. F. Wager, J. Appl. Phys. **75**, 3593 (1994).

Abu-Dayah, A., J. F. Wager, and S. Kobayashi, J. Appl. Phys. **74**, 5575 (1993).

Abu-Dayah, A.,S. Kobayashi, and J. F. Wager, Appl. Phys. Lett. **62**, 744 (1993).

Adachi, M., N. Takeuchi, S. Sakai, and H. Murakami, Phys. Stat. Sol. (a) **135**, K37 (1993).

Banovec, A., B. Stariha, A. Zalar, B. Pracek and M. Kern, Vacuum **41**, 1437 (1990).

Barrow, W., R. Coovert, E. Dickey, T. Flegal, M. Fullman, C. King and C. Laakso, Conference Record of the 1994 International Display Research Conference, 448 (1994).

Benoit, J., P. Benalloul, C. Barthou, S. Casette, and J. C. Soret, Phys. Stat. Sol. (a) **122**, 427 (1990).

Benoit, J., P. Benalloul, A. Geoffroy, N. Balbo, C. Barthou, J. P. Denis, and B. Blanzat, Phys. Stat. Sol. (a) **83**, 709 (1984).

Bhise, M. D., M. Katiyar, and A. H. Kitai, J. Appl. Phys. **67**, 1492 (1990).

Blackmore, J. M., and A. G. Cullis, Thin Solid Films **199**, 321 (1991).

Borisenko, N. D., M. F. Bulanyi, F. F. Kodzhespirov, and B. A. Polezhaev, J. Appl. Spectroscopy **55**, 911 (1992)

Bringuier, E., J. Appl. Phys. **66**, 1314 (1989).

Cattell, A. F.,B. Cockayne, K. Dexter, J. Kirton, and P. J. Wright, IEEE Transactions on Electron Devices **ED-30**, 471 (1983).

Cullity, B. D., Elements of X-ray Diffraction, 2nd edition (1978).

Douglas, A. A., J. F. Wager, D. C. Morton, J. B. Koh, and C. P. Hogh, J. Appl. Phys. **73**, 296 (1993).

Era, K., S. Shionoya, and Y. Washizawa, J. Phys. Chem. Solids **29**, 1827 (1968).

Falcony, C., M. Garcia, A. Ortiz, and J. C. Alonso, J. Appl. Phys. **72**, 1525 (1992).

Geoffroy, A., and E. Bringuier, J. Appl. Phys. **67**, 4276 (1990).

Georgobiani, A. N., L. S. Lepnev, and Y. A. Novikov, J. of Appl. Spectroscopy **42**, 511 (1985).

Higuchi, S., M. Ushio, Y. Nakanishi and K. Takahashi, Applied Surface science **33/34**, 667 (1988).

Hurd, J. M. and C. N. King, J. Electron. Mater. **8**, 879 (1979).

Husurianto, S., M. S. Thesis, Oregon State University, 1997.

Inoguchi, T., M. Takeda, Y. Kakihara, Y. Nakata and M. Yoshida, Digest of 1974 SID International Symposium, 84 (1974).

Kasai, P. H. and Y. Otomo, J. Chem. Phys. **37**, 1263 (1962)

Kennedy, T. A., E. R. Glaser, P. B. Klein, and R. N. Bhargava, Phys. Rev. B **52**, 14356 (1995).

Kreissel, J., Phys. Stat. Sol. (a) **97**, 191 (1986).

Li, J., W. Lu and Q. Shu, J. Luminescence **40**, 836 (1988).

Lindroos, S., T. Kanniainen, M. Leskela, E. Rauhala, Thin Solid Films **263**, 79 (1995).

Lu, X., M. S. Thesis, Oregon State University, 1998.

Mach, R. and G. O. Muller, Phys. Stat. Sol. (a) **81**, 609 (1984).

McArthur, R. C., J. D. Davidson, J. F. Wager, I. Khormaei, and C. N. King, Appl. Phys. Lett. **56**, 1889 (1990).

McClean, I. P., and C. B. Thomas, Semicond. Sci. Technol. **7**, 1394 (1992).

Migita, M., O. Kanehisa, M. Shiiki and H. Yamamoto, J. Cryst. Growth **93**, 686 (1988).

Mikami, A., K. Terada, K. Okibayashi, K. Tanaka, M. Yoshida and S. Nakajima, J. Cryst. Growth **110**, 381 (1991).

Mikami, A., K. Terada, K. Okibayashi, K. Tanaka, M. Yoshida, and S. Nakajima, J. Appl. Phys. **72**, 773 (1992).

Miller, R. T., M. S. Thesis, Oregon State University, 1995.

Nandagawe, J. K., P. K. Patil, P. R. Bote and R. D. Lawangar, Solid State Communications **77**, 513 (1991).

Nire, T., A. Matsuno, A. Miyakoshi, K. Ohmi, Jpn. J. Appl. Phys. **33**, 2605 (1994).

Oda, S., and H. Kukimoto, J. Luminescence **18/19**, 829 (1979).

Oikkonen, M., M. Blomberg, T. Tuomi, M. Tammenmaa, Thin Solid Films **124**, 317 (1985).

Ono, Y. A., Electroluminescent Displays, World Scientific, Singapore, 1995.

Ouyang, J., F. F. Fan, and A. J. Bard, J. Electrochem. Soc. **136**, 1033 (1989).

Pohl, U. W., and H. -E. Gumlich, Solid State Luminescence, edited by A. H. Kitai, Chapter 3. (1993).

Pohl, U. W., and H. -E. Gumlich, Phy. Rev. B **40**, 401194 (1989).

Sasakura, H., H. Kobayashi, S. Tanaka, J. Mita, T. Tanaka, and H. Nakayama, J. Appl. Phys. **52**, 6901 (1981).

Shih, S., P. D. Keir, and J. F. Wager, J. Appl. Phys. **78**, 5775 (1995).

Shih, S., P. D. Keir, J. Hitt, and J. F. Wager, Appl. Phys. Lett. **69**, 1921 (1996).

Suntola, T., Thin Solid Films **216**, 84 (1992).

Takeda, M., Y. Kanatani, H. Kishishita and H. Uede, Proc. SPIE 386, Advances in Display Technology III, 34 (1983).

Tammenmaa, M., H. Antson, M. Asplund, L. Hiltunen, M. Leskela, L. Niinisto, and E. Ristolainen, J. Crystal Growth **84**, 151 (1987).

Tanninen, V. P., M. Oikkonen and T. Tuomi, Thin Solid Films **109**, 283 (1983).

Theis, D., Phys. Stat. Sol. (a) **81**, 647 (1984).

Theis, D., H. Oppolzer, G. Ebbinghaus, and S. Schild, J. Cryst. Growth **63**, 47 (1983).

Thomas, A. E., G. J. Russell, and J. Woods, J. Phys. C: Solid State Phys. **17**, 6219 (1984).

Thomas, C. B., D. Sands, K. M. Brunson, and H. S. Reehal, J. Electrochem. Soc. **136**, 1235 (1989).

Thong, D. D., W. Heimbrodt, D. Hommel, and O. Goede, Phys. Stat. Sol. (a) **81**, 695 (1984).

Vlasenko, N.A., and Iu. A. Poplov, Optics & spectroscopy **8**, 39 (1960).

Wager, J. F., The 8th International Workshop on Electroluminescence, 33 (1996).

Weast, R. C., Handbook of Chemistry and Physics, B144 (1990).

Williamson, G. K., and W. H. Hall, Acta Metallurgica **1**, 22 (1953).

Warren, B. E., and B. L. Averbach, J. Appl. Phys. **21**, 595 (1950).

Xian, H., P. Benalloul, C. Barthou and J. Benoit, Thin Solid Films **248**, 193 (1994).

Zhang, Z., Z. Li, B. Mei, Z. Jiang, P. Wu, and S. Xu, Springer Proceeding in Physics, Vol. 38, edited by S. Shionoya and H. Kobayashi, p105 (1989).

Appendix

Appendix A.

Experimental Procedures for Depositing ZnS:Mn Thin Films

I. *Source Materials Preparation and HTCVD System Set-up.*

A. Making ZnS and Mn heaters: Ten feet of molybdenum and nichrome wire are used for making ZnS and Mn heaters, respectively. The wires are separated with nineteen 3-inch long ceramic tubes into which the wires are inserted. These tubes are then bound outside the 3 inch length graphite tube which have 1 inch inside diameter. Electrical insulating cement is put onto the tubes and baked in the oven at 90 °C for 2 hours to keep the wires from touching and to hold all the tubes together.

B. Place 15 gm ZnS and 5 gm Mn crucial material inside the individual heaters.

C. Use compressed nitrogen gas to clean out the particles in the reaction system.

D. Hook up the graphite tube to the heater and reaction chamber. Put the thermal insulating material around the heaters.

E. Insert two thermocouples with quartz tubes projecting into two heaters and the third thermocouple into the reaction chamber immediately beside the substrate holder to get accurate readings. K type thermocouples are used for this reactor system.

F. Plug the thermocouples (for ZnS, Mn and reaction chamber) onto the connector and the wires onto the power connector.

G. Close the flange evenly with screws at both ends of the stainless reactor tube. Connect all the tubes between the mass flow controller and the reaction chamber.

H. Check if valves are at right position.

1. "Process valve": Connect the reaction chamber to the pump system, "Rough valve": Connect the load luck chamber to pump system with the valve open.

2. "Process SGV" Connect the reaction chamber and load luck chamber with the valve closed.

II. Initial Start-up

A. Turn on the mechanical pump.

1. Turn on the control panel switch.

2. Turn the battle to a 30^{o} degree angle for about 10 minutes to optimize the pumping oil temperature.

3. Check the system pressure if below 30 torr.

B. Turn on the blower.

1. Turn on the power supply switch and pumping switch.

2. Turn on the blower if "foreline gauge" pressure is lower than 30 torr.

3. The system pressure must reach 10 torr within 5 minutes after cut-in.
4. After 1 hour, the system pressure must be lower than 0.1 torr. If not, check to see where the leakage is.
5. Pump the system for overnight (at least 10 hours).
6. Check to see if the system pressure is lower than 0.06 torr.
7. Turn on the cooling water.
8. Set the furnace temperature at 200 °C to help vacuum out the water vapor.

Note: Don't turn on the blower if the pressure is higher than 500 torr.

III. Deposition Preparation

A. Load substrate

1. Use compressed nitrogen gas to clean out the particles, if any, from the clean substrate.
2. Close the "Rough valve" to separate the loadlock chamber from the pumping system.
3. Vent the loadlock chamber to room pressure with high purity nitrogen gas.
4. Open the flange of the loadlock chamber.
5. Place the substrate on the graphite-made substrate holder in correct position.

6. Close the flange of the loadlock chamber.

7. Close the "Process valve" to isolate the reaction chamber.

8. Turn off the blower.

9. Turn on the "Rough valve" to allow the mechanical pump on the loadlock chamber to work.

10. Turn on the blower if "foreline gauge" pressure is lower than 30 torr.

11. When the system pressure is about the same as the pressure of the loadlock chamber, open the "process valve".

    Note: The glass substrate should be loaded at least 2 hours before deposition in order to clean the substrate surface.

B. Increase the furnace temperature.

Increase the 3-zone furnace temperature gradually to the setpoint. If a substrate temperature of 550 °C is chosen, zone 1 (at the right position) is set at 650 °C, and zones 2 and 3 are set at 500 °C. It takes about one and half hours to reach the setpoint. The temperature is monitored by a furnace thermocouples and three thermocouples in the reactor.

C. Increase heater temperature.

Increase the ZnS heater and Mn heater temperatures gradually by the Variac power supply. For the ZnS heater, increase up to forty scale every 10 readings of Variac. After that, reduce the to 7-5 scales depending on how fast the temperature reading increases.

D. Clean away the loose ZnS and Mn powder and particles.

1. Set the purging nitrogen gas flow rate. For the ZnS heater, set it at 10 sccm higher than the experimental setpoint. For Mn heater, set it at 1 sccm higher than the experimental setpoint.
2. When the ZnS heater temperature is up to 800 °C, close the "gate valve" and "rough valve".
3. Turn on two mass flow controllers for 5 min.

   Note: During purging, "Rough Valve" and "Gate Valve" should both be closed to prevent the powder blowing into the loadlock chamber and sticking on the glass.
4. Adjust the mass flow controller setpoint back to the experimental setpoint.

E. By-pass the residual argon gas, which fills in the tube and mass flow controller, controlling with HCl gas.

1. Close the process valve and rough valve (or check to see if they are closed).
2. Open the first valve, close to pump system on the by-pass tube.
3. Open the second valve on the by-pass tube.
4. Force the mass flow controller fully open by plugging in a specific connector.
5. Check the foreline pressure if there is still is gas in the by-pass tube.

6. Open the process valve and roughing valve.

7. Take out the specific connector.

8. Fill the tube with hydrogen chloride gas.

F. Load the substrate in the reaction chamber.

1. Open the gate valve and roughing valve.

2. Put a very small amount of vacuum grease on the rod to lubricate it to prevent the reactor leaking from the hole.

3. Push the rod into the reactor slowly. (Check to see if it leaks while pushing)

4. Before reaching the final position (about 3~4 inches), rotate the rod to a 30° degree angle to the operator. Then push into the correct position.

G. Increase heater temperatures to the experimental setpoints.

H. Adjust zone 2 and 3 furnace temperature to the experimental setpoint.

Note: The substrate temperature on the monitor reading will decrease due to the cool substrate holder which has been moved inside. Then start increasing after loading the substrate holder 10-12 minutes later. At this time, zones 2 and 3 should be adjusted to lower temperatures to reach the experimental setpoints if the experimental substrate temperature is 550°C.

IV. Deposition

A. Open the tanks valves.

B. Turn on the mass flow controllers.

C. Deposit thin film for desired time.

V. Ending deposition

A. Turn off the mass flow controllers.

B. Decrease the heaters and furnace temperatures gradually.

1. Decrease the heater temperatures slowly.

2. After finishing step 1, decrease furnace temperature gradually.

C. Slowly pull out the substrate holder to the loadlock chamber.

Note: Be careful. Prevent leaking from the connection point where the rod can be pulled out. Prevent the O-ring from burning due to the hot rod. It takes about 1/2 hour to pull the substrate holder out to the loadlock chamber.

D. Close the gate valve and roughing valve (to separate the loadlock chamber from the reactor).

E. Purge the pure nitrogen gas (5N grade) into the loadlock chamber to cool the substrate holder. It takes 1 to 1 and 1/2 hours to cool down to around 40-50 ^{o}C temperature.

F. Take out the sample.

Note: The procedure is the same as step A: "Load Substrate" in procedure III-deposition preparation, but only involves taking out the sample instead of loading the substrate. After taking out the sample, the loadlock

chamber should be closed again to prevent water vapor absorption on the wall.

G. By-pass the HCl gas which resided in the tube and in the mass flow controller. The procedure is the same as Step E. in Procedure III "Deposition Preparation" (But fill the mass flow controller with argon gas instead of hydrogen chloride gas after purging).

H. System shutdown for short term (overnight) -- waiting for next run.

1. Turn off heaters power, furnace power, and cooling water.
2. If there is enough ZnS and Mn source remaining, do not turn off the pumping system.

I. System shutdown for long term (for a weekend or a whole week)

1. Turn off heater power, furnace power, and cooling water.
2. Shut off the blower and keep the mechanical pump running until the preparation for the next run is ready.

Note: The system should be kept pumping to reduce water vapor absorption inside the reactor even while not doing the experiment.

The hydrogen chloride gas left in tube and mass flow controller should be vacuumed out of the by-pass tube. The tube should be filled with nitrogen or argon gas when the experiment is finished or not running, or the tube and mass flow controller will be destroyed.